UNIVERSITY OF CALIFORNIA, SAN DIEGO

BIOMECHANICS OF OSTEOCHONDRAL GRAFT INSERTION: CARTILAGE DAMAGE AND PROTECTION STRATEGIES

A dissertation submitted in partial satisfaction of the

requirements for the degree Doctor of Philosophy

in

Materials Science and Engineering

by

Wei-i Alvin Su

Committee in charge:

Professor Robert L. Sah, Chair
Professor William D. Bugbee
Professor Shengqiang Cai
Professor Koichi Masuda
Professor Jeffery H. Omens

2014

The dissertation of Wei-i Su is approved, and it is acceptable in quality and form for publication on microfilm and electronically:

_____

_____

_____

_____

_____

_____

Chair

University of California, San Diego

2014

TABLE OF CONTENTS

LIST OF FIGURES AND TABLES

ACKNOWLEDGMENTS

I would like to thank and acknowledge my mentors, friends and family who have been with me throughout the years. I could have never accomplished this dissertation work without your support, encouragement and faith.

I would like to express my sincere gratitude to my advisor, Dr. Robert Sah, who has been enthusiastically sharing his wisdom in science and engineering, as well as infinitely polishing me toward a better self. In my continued development as a clinician scientist, I will bear in mind the philosophy of "everything is possible" and the spirit to pursue the perfection that always seems one step away. I would also like to thank Dr. William Bugbee, for his visionary perspectives in future directions of this work, and his practical advices for my career.

I would also like to thank the other professors in my committee, Dr. Jeffery Omens, Dr. Koichi Masuda and Dr. Shengqiang Cai for their support and helpful advice.

I would like to acknowledge National Yang-Ming University and Taipei Veterans General Hospital, Taiwan, for the edification, education and training that introduced me to the beautiful world of medicine and science.

I would like to acknowledge all the wonderful people with whom I have spent good times together inside and outside the lab. I am happy to see the undergraduate students, who spent countless days and nights with me to accomplish these projects, Yunchan Chen, Dustin Wailes and Yao Dong, move forward to the next stages of their lives. I would like to remark on how lucky I am to have Dr. Andrea Pallante-Kichura as a friend. Her invaluable insights and wisdom shed light on my toughest days in

graduate school. I would like to also thank Dr. Albert Chen, Van Wong and Dr. Michele Temple-Wong for their strong support in resolving both theoretical and technical issues in research.

Last but not least, I am incredibly grateful to the angels, the light in my life – my family, especially my wife Sophie Shuaichun Lin, my parents and my two kids, Elpis and Triton. Thank you for bearing with my absence from time to time, and your endless love that have carried me through all the challenges while juggling the roles of a good father, a thoughtful son, a sweet husband and a trustworthy graduate student.

Chapter 2 has been submitted in full to *Journal of Biomechanics*, Su, Alvin W.; Chen, Yunchan; Dong, Yao; Wailes, Dustin H.; Wong, Van W.; Cai, Shengqiang; Chen, Albert C.; Bugbee, William D.; Sah, Robert L., 2014. The dissertation author was the primary investigator and author of this paper.

Chapter 3 has been submitted in full to *The American Journal of Sports Medicine*, Su, Alvin W.; Chen, Yunchan; Wailes, Dustin H.; Wong, Van W.; Cai, Shengqiang; Chen, Albert C.; Bugbee, William D.; Sah, Robert L., 2014. The dissertation author was the primary investigator and author of this paper.

VITA

2004	M.D. National Yang-Ming University, Taipei, Taiwan
2005-2009	Residency Department of Orthopaedic Surgery Taipei Veterans General Hospital, Taiwan
2009-2010	Chief Resident Department of Orthopaedic Surgery Taipei Veterans General Hospital, Taiwan
2010-2011	Clinical Fellowship Adult Reconstruction & Musculoskeletal Tumor Department of Orthopaedic Surgery Taipei Veterans General Hospital, Taiwan
2011-2014	Graduate Student Researcher Cartilage Tissue Engineering Laboratory University of California, San Diego, La Jolla, California
2014	Ph.D., Materials Science and Engineering University of California, San Diego, La Jolla, California

Journal Articles

Lin CJ, Chiang CC, Wu PK, Chen CF, Huang CK, Su AW, *Chen WM, Liu CL, Chen TH. Effectiveness of plate augmentation for femoral shaft nonunion after nailing. *J Chin Med Assoc*. 2012;75(8):396–401.

Chen CM, *Su AW, Chiu FY, Chen TH. A surgical protocol of ankle arthrodesis with combined Ilizarov's distraction-compression osteogenesis and locked nailing for osteomyelitis around the ankle joint. *J Trauma*. 2010;69(3):660–665.

Su AW, Chen CF, Huang CK, Chen PCH, *Chen WM, Chen TH. Primary hyperparathyroidism with brown tumor mimicking metastatic bone malignancy. *J Chin Med Assoc*. 2010;73(3):177–180.

Su AW, *Chen WM, Chen CF, Chen TH. Innovative trident fixation technique for allograft knee arthrodesis for high-grade osteosarcoma around the knee. *Jpn J Clin Oncol*. 2009;39(11):739–744.

Selected Abstracts

Su AW, Chen Y, Dong Y, Wailes DH, Wong VW, Chen AC, Bugbee WD, Sah RL. Mechanical Mediators of Cartilage Damage During Impact: Energy Density and Shear. *Trans Orthop Res Soc 39, 1076*, 2014.

Wailes DH, Su AW, Chen Y, Wong VW, Chen AC, Sah RL. Spatial Variation of Cell Death after Articular Cartilage Impact. *UC San Diego School of Medicine Independent Study Project Presentation*, 2013.

Mukherjee S, Maheshwari AJ, Su AW, Cory E, Chen AC, Sah RL. Model for Repair of Focal Cartilage Defect with Immature Osteochondral Graft. *NIH Short-Term Research Training Grant Presentation*, 2012.

Su AW, Liu Y. Long Term Results of Scaphoid Nonunion Treated by Bone Grafting and Herbert's Screw Fixation – A report of follow-up more than 5 years. *Taiwan Orthopedic Association Annual Meeting*, 2006

ABSTRACT OF THE DISSERTATION

BIOMECHANICS OF OSTEOCHONDRAL GRAFT INSERTION:

CARTILAGE DAMAGE AND PROTECTION STRATEGIES

by

Wei-i Alvin Su

Doctor of Philosophy in Materials Science and Engineering

University of California, San Diego, 2014

Professor Robert L. Sah, Chair

Osteochondral graft repair is one of the most effective surgical treatments for focal cartilage defects. During such surgery, the load applied on the graft during impact insertion can result in damage to its articular cartilage, and therefore be

detrimental to long-term effectiveness and clinical outcome. The exact mechanical stimuli by which impact loading causes such damage are unknown, with suggested and known mechanobiological factors and mediators including compressive stress, compressive strain, impulse, and energy density.

Three hypotheses regarding osteochondral graft (OCG) insertion were tested in the dissertation. (1) Energy delivered to the graft is the critical biomechanical determinant of cartilage damage during impact. (2) Increasing tightness of graft-host fit leads to higher insertion energy and resultant cartilage damage. (3) Modifying the geometry of the graft can alter the mechanics of impact insertion and therefore provides cartilage protection by reducing energy delivery to the graft.

Osteochondral sample (OCS) or osteochondral graft (OCG), as well as osteochondral recipient site (OCR), were harvested fresh from distal femora of adult bovine. An instrumented drop tower apparatus was used to apply a range of energy and to quantify energy delivered to samples, as well as a variety of other mechanical factors, during impact of OCS, or insertion of OCG into OCR. Damage to the articular cartilage was quantified as total crack length and viability of chondrocytes at the articular surface.

During OCS impact and OCG insertion into OCR, the resultant damage to graft articular cartilage was affected by the delivered energy. (1) Delivered energy was decreased when a cushion was inserted between the drop mass and OCS, and total crack length of the cartilage surface was strongly correlated with delivered energy. (2) Higher tightness of graft-host fit resulted in higher cumulative energy delivered to the graft during insertion, as well as more cartilage damage. (3) With same tightness of fit, the OCG with modified geometry led to less energy delivery to the graft during insertion, with less resultant damage to cartilage.

The experimental approach may be applied to a variety of impact insertion scenarios. The use of a cushion altered impact mechanics, mimicking certain aspects of graft insertion, and may be relevant to injury scenarios. Understanding the relationships between graft-host tightness of fit, graft geometry, and osteochondral graft insertion biomechanics may facilitate design for improved surgical instruments.

CHAPTER 1

INTRODUCTION

1.1 General Introduction to the Dissertation

Articular cartilage is susceptible to impact injury and has limited healing potential. Focal cartilage defects are commonly located in weight-bearing areas of the joint, and are usually symptomatic. Such lesions can progress in size and depth and lead to development of osteoarthritis. Surgical intervention is often required to alleviate pain and restore joint function for the patients, as well as to minimize the progression of the lesion. Osteochondral graft (OCG) repair is one of the most effective treatment options for focal cartilage defect. During surgery, the surgeon applies multiple impact taps to insert the OCG into the OCR. Such an impact insertion procedure can result in damage to articular cartilage of OCG, and be deleterious to the clinical outcome.

The overall motivation of this dissertation was: (a) to advance the understanding of biomechanics and the mechanobiological consequences of OCG impact insertion, (b) to develop potential strategies to preserve articular cartilage health during the surgical procedure and benefit clinical outcome. *Ex vivo* studies were conducted using adult bovine knee joints, a useful large animal model that provides solid base for future translational investigations. The objectives of this dissertations were: (1) to determine the critical biomechanical mediators for impact injury to OCG,

(2) to determine the effect of graft-host interference fit on biomechanics of OCG insertion, (3) to develop potential strategies to minimize damage to graft cartilage during OCG insertion, (4) to provide an innovative impact delivery system for studies of traumatic injury to osteochondral samples.

Chapter 1 of the dissertation starts with a review of the important role of OCG repair in clinical management of cartilage defects, current issues about the surgical procedure, and the problems to be solved from bedside-to-bench perspectives. The chapter continues by discussing the background of the translational research problems from the aspects of biomechanics and mechanobiology.

Chapter 2, which has been submitted in full to *Journal of Biomechanics*, introduces delivered energy density as one of the critical biomechanical determinant of damage to articular cartilage. This chapter utilizes a specialized impact load delivery system with a drop tower apparatus and a cushion material, providing an innovative approach to study traumatic injury to osteochondral samples.

Chapter 3, which has been submitted in full to *The American Journal of Sports Medicine*, examines the effect of graft-host interference fit on OCG insertion biomechanics and the resultant damage to the cartilage of the graft. This chapter also describes strategies to minimize such damage by modifying subchondral bone geometry of the OCG.

Finally, **Chapter 4** summarizes the major findings and discusses future directions and potential bench-to-bedside applications of this work.

1.2 Clinical Perspectives of Osteochondral Graft Repair Surgery

Articular cartilage has limited healing potential and is susceptible to damage caused by traumatic injury. The trauma can lead to partial-thickness or full-thickness focal cartilage defects [1], or intra-articular fracture [2]. Focal cartilage defects in the weight-bearing region of the joint are common [3, 4]. These lesions are usually symptomatic, resulting in pain and limited function of the joint [5, 6]. If left untreated, such defects can progress in size [7] and lead to osteoarthritis [8], causing further disability to the patient. Surgical intervention is often indicated to alleviate clinical symptoms and disease progression.

OCG repair is one of the most effective surgical treatments for focal articular cartilage defects [9, 10]. Autologous OCG is best for smaller defects that have surface area generally less than 2 cm^2.due to limited donor tissue availiability. The graft can be up to 10 mm in diameter and 12 to 15 mm in length. Allogenic OCG is ideal for larger defects, and can be larger in diameter than autologous OCG, but shorter (6 to 8 mm) in length to minimize immunologic response at the bone contact surface with the host tissue [10, 11]. Insertion is typically accomplished by applying impact load to the articular cartilage of the OCG and may result in chondrocyte death [12]. Fixation of both types of OCG depend on certain amount of press fit with the OCR. Additional internal fixation with bioabsorbable or metal screws may be used to enhance graft stability, especially for huge allogenic OCG [10, 11]. Viable chondrocytes and cartilage matrix integrity are important for clinical success of the surgery [13, 14].

Understanding the mechanobiological factors that cause impact injury to the cartilage facilitates development of strategies to preserve cartilage health. Two features of impact damage to cartilage damage are fissure formation [15-17] and chondrocyte death [15, 18-20]. Modification of OCG repair surgical procedures or

instrument design may minimize damage to articular cartilage of the graft and benefit clinical outcome of the patients.

1.3 Biomechanics of Osteochondral Graft Insertion

One of the key steps of osteochondral graft repair surgery is impact insertion of the OCG into the OCR. Understanding the biomechanics during such insertion process facilitates surgical procedure and instrument design, and may therefore improve the clinical outcome. The biomechanics of insertion involves graft-host interaction during OCG advancement, and therefore requires considerations in addition to isolated osteochondral or cartilage sample impact mechanics.

The surgeon typically applies multiple taps to complete the insertion, and peak contact force of each tap increases gradually as the OCG advances into the OCR. This was shown by using adult bovine model, either with graft diameter of 4.6 mm [21] or 8.0 mm [22]. Similarly, the insertional load increases when a metal nail is tapped deeper into the wood, and such process involves elastic deformation of both parts and plastic deformation mainly of the wood [23]. The graft-host interaction during OCG insertion into OCR may involve elastic and plastic deformation, as well as possible microfracture of the subchondral bones at the interface. Therefore, higher impact load may be required to further advance the graft from a deeper position.

The time duration of each tap is brief. The typical measure of this is the duration between the two half maximal values of the peak contact force. This tap duration has been reported to be as short as 0.56 ms [12] or less than 1 ms [24] in human *ex vivo* model, 2.71 ms during *in vivo* surgery for goat [14], or approximately 5 ms in an adult bovine model [22]. The biomechanical results of applying rapid, instantaneous impact load on isolated osteochondral samples may thus provide insights on OCG insertion biomechanics due to similar brief duration of the applied load.

When the OCG "bottoms out", that is, when the OCG base first contacts the corresponding base of the OCR, peak contact force of each tap increases. Such bottoming out occurs normally if an OCG is longer than the corresponding OCR and the OCG is inserted until approximately flush with the OCR surface. In contrast, if an OCG is the same length or shorter than the OCR, bottoming out occurs if the graft is placed to be slightly recessed at completion of insertion. *should describe a bit of what level of OCG vs OCR surfaces are targeted, before the sentence before* Bottoming out the OCG results in substantial increase of the axial load in human *ex vivo* model [24, 25] or adult bovine model [21]. Such axial load is higher in shorter OCG due to higher structural stiffness [25]. Bottoming out or recessive seating of the OCG may be associated with better graft stability and graft-host healing after insertion. However, the resultant high amplitude loading of the final taps may jeopardize cartilage health of the OCG.

Sufficient graft stability is crucial to clinical success of OCG repair surgery [26, 27]. Clinically, the OCG sustains compressive and shearing load after surgery. Experimentally, the issue of graft stability has been approached by measuring the pull-out strength after OCG insertion in an *ex vivo* porcine model [28]. The pull-out strength increases with OCG length and diameter and decreases with repeated insertion. Another porcine model showed that after insertion, both pull-out and push-in strength decreases after seven days of *in vitro* incubation, compared to samples measured on the same day of insertion [29], suggesting a possible decrease in graft stability in the week following surgery. It should be noticed that the graft-host healing response *in vivo* is not identical to that in the *in vitro* incubation model. The stress relaxation of the subchondral bone needs to be considered as well.

The graft-host interference fit between OCG and OCR can be an important consideration in surgical instrument design. Certain studies have reported the possible effect of interference on analogous situations of insertion. The insertional load is higher when driving nails of larger diameter into the wood [23]. The interference that exceeds the elastic limits of the inserted and the recipient parts leads to higher resistance to relative motion [30]. Tighter fit may be beneficial to graft-host healing due to better post-insertional graft stability, but at the same time may require higher impact energy to complete the insertion. The effect of interference fit on insertion biomechanics and the resultant tissue damage has not been reported.

1.4 Impact Mechanics of Articular Cartilage

The material response of articular cartilage under axial load involves the type of load applied, the structure of the cartilage tissue as well as boundary conditions such as circumferential confinement of the tissue. The impact load applied to articular cartilage, such as that during OCG insertion into OCR, is typically instantaneous with minimal fluid exudation. Instantaneous deformation of cartilage disc is anisotropic and depends on collagen orientation. Under the same axial stress, the diameter deformation of human femoral head cartilage discs is more in the direction perpendicular to the articular cartilage split lines, and less in that parallel to the split lines. Such deformation increases with the applied axial stress, and decreases when the subchondral bone is attached to the cartilage samples [31]. Thus, the impact mechanics of OCG may be different from that of isolated cartilage samples.

Articular cartilage as a viscoelastic biological tissue, commonly modeled as a biphasic material, is composed of fluid and solid phases [32]. Under unconfined compression, the applied load is initially supported mostly by pressurization of the fluid phase, which is restricted from instantaneous movement relative to the solid matrix. The load is also partially supported by the elastic deformation of the solid phase of cartilage. Since there is minimal fluid exudation, cartilage volume is conserved and lateral strain (expansion) is approximately half of the axial strain (compression). Stress relaxation of cartilage in this unconfined compression situation involves fluid exudation and decreased lateral expansion. As the load is sustained, fluid exudes from the periphery, and the radial recoil of the solid phase causes a decrease in the lateral expansion of the cartilage [33, 34].

Instantaneous load with sufficient amplitude can cause gross cracks in cartilage. When the load was applied rapidly enough, the articular cartilage absorbs

the applied load predominantly by crack formation. Axial strain of 30% and 50% applied with strain rate 1000 s^{-1} both results in cartilage cracks perpendicular to articular surface in human osteochondral plugs [15]. Higher axial strain results in longer, deeper cracks. Total applied energy of 0.49 J led to cracks in adult bovine cartilage discs 5 mm in diameter [16]. Such cracks are mostly 45 degrees to the articular surface, and extend only to the middle zone of cartilage. In addition, higher stress rate (900 MPa/s) is associated with more cracks compared to lower stress rate (40 MPa/s) in adult bovine cartilage discs 6.35 mm in diameter [17]. The formation of 45 degree cracks may be explained by shear strain mechanism, which results in two deviatoric strain components both diagonal to the axial compressive load. The perpendicular cracks in human samples may be due to the customized experimental settings. Cartilage can be compressed from articular surface to only a certain depth, and the rest of the cartilage was confined in the metal chamber.

Higher total applied energy results in higher energy delivered to, as well as dissipated by, isolated cartilage discs [35]. The impact energy was delivered to adult bovine cartilage discs using a drop tower apparatus. Force-displacement measurements allow determination of energy delivery and dissipation. Higher ratio of energy dissipation implies a more plastic material response [36], and may be associated with more cartilage matrix damage.

1.5 Impact Mechanobiology of Articular Cartilage

Impact insertion of OCG during real surgery can cause chondrocyte death. Insertion of human OCG (15 mm in diameter) *ex vivo* by standard surgical procedures resulted in more cell death 48 hours after insertion, compared to the non-loaded OCG [12]. With impaction of human OCG, chondrocyte death increases with load magnitude [24]. Cell death aggregates at the superficial zone [12, 24] and spreads deeper into the articular cartilage [20, 37].

Impact insertion of OCG using a large number of gentle taps preserves cell viability. Cell death is correlated with mean impact force, but not with number of impact taps in porcine and bovine models [21]. When applying the same total impact impulse of 7 N•s, lower load magnitude coupled with more taps leads to higher chondrocyte viability, compared to higher load magnitude with less taps [24].

Previous studies have used isolated osteochondral samples to assess mechanobiology of impact injury to articular cartilage. Various mechanical factors during impact have been suggested to cause cartilage damage. Chondrocyte death is associated with impact force [21, 24, 37], contact stress [15, 19], compressive stress rate [17, 38], compressive strain [15, 39], compressive strain rate [40], and total impact energy [20, 35, 41]. Early intervention using biochemical agents such as caspase-inhibitors [42, 43] or anti-oxidative agents [44, 45] may improve chondrocyte survival after impact.

Chondrocyte death increases with total applied energy. Depth of cell death is associated with the energy delivered by a spring device [21], or by a drop tower apparatus [20]. Sufficient applied energy results in fracture of the cartilage [20]. The material toughness to create fracture in the same plane for adult canine articular cartilage is 0.14 to 1.50 mJ/mm^2 [46], and that of adult bovine to shear the cartilage

off the subchondral bone is 36 to 58 mJ/mm^2 [47]. Damage to articular cartilage involves energy dissipation for viscoelasticity, friction, plastic deformation as well as creation of free surfaces [48]. Therefore, strategies altering impact mechanics and consequent energy distribution may decrease damage to articular cartilage.

1.6 References

1. Mandelbaum BR, Browne JE, Fu F, Micheli L, Mosely JB, Jr., Erggelet C, Minas T, Peterson L. Articular cartilage lesions of the knee. *Am J Sports Med*. 1998;26(6):853-861.

2. Trumble T, Allan CH, Miyano J, Clark JM, Ott S, Jones DE, Fernacola P, Magnusson M, Tencer A. A preliminary study of joint surface changes after an intraarticular fracture: a sheep model of a tibia fracture with weight bearing after internal fixation. *J Orthop Trauma*. 2001;15(5):326-332.

3. Curl WW, Krome J, Gordon ES, Rushing J, Smith BP, Poehling GG. Cartilage injuries: a review of 31,516 knee arthroscopies. *Arthroscopy*. 1997;13:456-460.

4. Hjelle K, Solheim E, Strand T, Muri R, Brittberg M. Articular cartilage defects in 1,000 knee arthroscopies. *Arthroscopy*. 2002;18(7):730-734.

5. Martin JA, Buckwalter JA. Post-traumatic osteoarthritis: the role of stress induced chondrocyte damage. *Biorheology*. 2006;43(3-4):517-521.

6. Buckwalter JA, Martin JA, Brown TD. Perspectives on chondrocyte mechanobiology and osteoarthritis. *Biorheology*. 2006;43(3-4):603-609.

7. Cicuttini F, Ding C, Wluka A, Davis S, Ebeling PR, Jones G. Association of cartilage defects with loss of knee cartilage in healthy, middle-age adults: a prospective study. *Arthritis Rheum*. 2005;52(7):2033-2039.

8. Shelbourne KD, Jari S, Gray T. Outcome of untreated traumatic articular cartilage defects of the knee: a natural history study. *J Bone Joint Surg Am*. 2003;85-A Suppl 2:8-16.

9. Hangody L, Vasarhelyi G, Hangody LR, Sukosd Z, Tibay G, Bartha L, Bodo G. Autologous osteochondral grafting--technique and long-term results. *Injury*. 2008;39 Suppl 1:S32-39.

10. Cole BJ, Pascual-Garrido C, Grumet RC. Surgical management of articular cartilage defects in the knee. *J Bone Joint Surg Am*. 2009;91(7):1778-1790.

11. Alford JW, Cole BJ. Cartilage restoration, part 2: techniques, outcomes, and future directions. *Am J Sports Med*. 2005;33(3):443-460.

12. Borazjani BH, Chen AC, Bae WC, Patil S, Sah RL, Firestein GS, Bugbee WD. Effect of impact on chondrocyte viability during the insertion of human osteochondral grafts. *J Bone Joint Surg Am*. 2006;88:1934-1943.

13. Pallante-Kichura AL, Cory E, Bugbee WD, Sah RL. Bone cysts after osteochondral allograft repair of cartilage defects in goats suggest abnormal interaction between subchondral bone and overlying synovial joint tissues. *Bone*. 2013;57:259–268.

14. Pallante AL, Chen AC, Ball ST, Amiel D, Masuda K, Sah RL, Bugbee WD. The in vivo performance of osteochondral allografts in the goat is diminished with extended storage and decreased cartilage cellularity. *Am J Sports Med*. 2012;40:1814-1823.

15. Repo RU, Finlay JB. Survival of articular cartilage after controlled impact. *J Bone Joint Surg Am*. 1977;59-A:1068-1076.

16. Jeffrey JE, Gregory DW, Aspden RM. Matrix damage and chondrocyte viability following a single impact load on articular cartilage. *Arch Biochem Biophys*. 1995;322:87-96.

17. Ewers BJ, Dvoracek-Driksna D, Orth MW, Haut RC. The extent of matrix damage and chondrocyte death in mechanically traumatized articular cartilage explants depends on rate of loading. *J Orthop Res*. 2001;19:779-784.

18. Loening A, Levenston M, James I, Nuttal M, Hung H, Gowen M, Grodzinsky A, Lark M. Injurious mechanical compression of bovine articular cartilage induces chondrocyte apoptosis. *Arch Biochem Biophys*. 2000;381:205-212.

19. Torzilli PA, Grigiene R, Borrelli J, Jr., Helfet DL. Effect of impact load on articular cartilage: cell metabolism and viability, and matrix water content. *J Biomech Eng*. 1999;121:433-441.

20. Szczodry M, Coyle CH, Kramer SJ, Smolinski P, Chu CR. Progressive chondrocyte death after impact injury indicates a need for chondroprotective therapy. *Am J Sports Med*. 2009;37(12):2318-2322.

21. Whiteside RA, Jakob RP, Wyss UP, Mainil-Varlet P. Impact loading of articular cartilage during transplantation of osteochondral autograft. *J Bone Joint Surg Br*. 2005;87:1285-1291.

22. Pylawka TK, Wimmer M, Cole BJ, Virdi AS, Williams JM. Impaction affects cell viability in osteochondral tissues during transplantation. *J Knee Surg*. 2007;20:105-110.

23. Salem SA, Al-Hassani ST, Johnson W. Aspects of the mechanics of driving nails into wood. *Int J Mech Sci*. 1975;17:211-225.

24. Patil S, Butcher W, D'Lima DD, Steklov N, Bugbee WD, Hoenecke HR. Effect of osteochondral graft insertion forces on chondrocyte viability. *Am J Sports Med*. 2008;36(9):1726-1732.

25. Kock NB, van Susante JL, Wymenga AB, Buma P. Press-fit stability of an osteochondral autograft: Influence of different plug length and perfect depth alignment. *Acta Orthop*. 2006;77:422-428.

26. Berlet GC, Mascia A, Miniaci A. Treatment of unstable osteochondritis dissecans lesions of the knee using autogenous osteochondral grafts (mosaicplasty). *Arthroscopy*. 1999;15:312-316.

27. Kish G, Modis L, Hangody L. Osteochondral mosaicplasty for the treatment of focal cartilage and osteochondral lesions of the knee and talus in the athlete. Rationale, indications, techniques, and results. *Clin Sports Med*. 1999;18:45-66, vi.

28. Duchow J, Hess T, Kohn D. Primary stability of press-fit-implanted osteochondral grafts. *Am J Sports Med*. 2000;28:24-27.

29. Whiteside RA, Bryant JT, Jakob RP, Mainil-Varlet P, Wyss UP. Short-term load bearing capacity of osteochondral autografts implanted by the mosaicplasty technique: an in vitro porcine model. *J Biomech*. 2003;36(8):1203-1208.

30. Selvage CC. *Assembly of interference fits by impact and constant force methods*, Massachusetts Institute of Technology; 1979.

31. Mizrahi J, Maroudas A, Lanir Y, Ziv I, Webber TJ. The "instantaneous" deformation of cartilage: effects of collagen fiber orientation and osmotic stress. *Biorheology*. 1986;23:311-330.

32. Mow VC, Kuei SC, Lai WM, Armstrong CG. Biphasic creep and stress relaxation of articular cartilage in compression: theory and experiment. *J Biomech Eng*. 1980;102(1):73-84.

33. Armstrong CG, Lai WM, Mow VC. An analysis of the unconfined compression of articular cartilage. *J Biomech Eng*. 1984;106:165-173.

34. Wong M, Ponticiello M, Kovanen V, Jurvelin JS. Volumetric changes of articular cartilage during stress relaxation in unconfined compression. *J Biomech*. 2000;33(9):1049-1054.

35. Burgin LV, Aspden RM. Impact testing to determine the mechanical properties of articular cartilage in isolation and on bone. *J Mater Sci Mater Med*. 2008 19:703-711.

36. Stronge WJ. Rigid body collisions with friction. *Proc R Soc Lond A*. 1990;431(1881):169-181.

37. Kang RW, Friel NA, Williams JM, Cole BJ, Wimmer MA. Effect of impaction sequence on osteochondral graft damage: the role of repeated and varying loads. *Am J Sports Med*. 2010;38(1):105-113.

38. Milentijevic D, Torzilli PA. Influence of stress rate on water loss, matrix deformation and chondrocyte viability in impacted articular cartilage. *J Biomech*. 2005;38:493-502.

39. Torzilli PA, Deng XH, Ramcharan M. Effect of compressive strain on cell viability in statically loaded articular cartilage. *Biomech Model Mechanobiol*. 2006;5(2-3):123-132.

40. Quinn TM, Allen RG, Schalet BJ, Perumbuli P, Hunziker EB. Matrix and cell injury due to sub-impact loading of adult bovine articular cartilage explants: effects of strain rate and peak stress. *J Orthop Res*. 2001;19:242-249.

41. Finlay JB, Repo RU. Energy absorbing ability of articular cartilage during impact. *Med Biol Eng Comput*. 1979 17:397-403.

42. D'Lima DD, Hashimoto S, Chen PC, Lotz MK, Colwell CW, Jr. Prevention of chondrocyte apoptosis. *J Bone Joint Surg Am*. 2001;83-A Suppl 2(Pt 1):25-26.

43. D'Lima D, Hermida J, Hashimoto S, Colwell C, Lotz M. Caspase inhibitors reduce severity of cartilage lesions in experimental osteoarthritis. *Arthritis Rheum*. 2006;54(6):1814-1821.

44. Kurz B, Lemke A, Kehn M, Domm C, Patwari P, Frank EH, Grodzinsky AJ, M S. Influence of tissue maturation and antioxidants on the apoptotic response of articular cartilage after injurious compression. *Arthritis Rheum*. 2004;50:123-130.

45. Martin JA, McCabe D, Walter M, Buckwalter JA, McKinley TO. N-acetylcysteine inhibits post-impact chondrocyte death in osteochondral explants. *J Bone Joint Surg Am*. 2009;91:1890-1897.

46. Chin-Purcell MV, Lewis JL. Fracture of articular cartilage. *J Biomech Eng*. 1996;118:545-556.

47. Broom ND, Oloyede A, Flachsmann R, Hows M. Dynamic fracture characteristics of the osteochondral junction undergoing shear deformation. *Med Eng Phys*. 1996;18:396-404.

48. Ahsan T, Sah RL. Fracture mechanics characterization of integrative cartilage repair using the T-peel test. Paper presented at: Trans Orthop Res Soc1996.

CHAPTER 2

BIOMECHANICS OF OSTEOCHONDRAL IMPACT: EFFECT OF CUSHIONING ON CARTILAGE DAMAGE

2.1 Abstract

Articular cartilage is susceptible to impact injury and the resultant damage may lead to development of osteoarthritis. The exact mechanical stimuli causing such damage are unknown, with suggested and known mechanobiological factors and mediators including compressive stress, compressive strain, impulse, and energy density. We tested the hypothesis that energy density delivered to the sample (ϱ^{OCS}) is the most critical biomechanical determinant of cartilage damage during impact to osteochondral samples. A specialized drop tower apparatus with an optional cushion was used to generate a range of ϱ^{OCS} as well as a variety of other mechanical factors. Damage to the articular cartilage quantified by total crack length and overall surface chondrocyte viability was strongly correlated with ϱ^{OCS}. Quantification of the contact force and concomitant compressive displacement provided insight of modeling the biomechanics of osteochondral samples sustaining impact load. Presence of the cushion provided an innovative approach to study impact scenarios with additional

component for energy partitioning in the system, such as osteochondral graft insertion to repair cartilage defect, or soft tissue interposition during traumatic accidents.

2.2 Introduction

Articular cartilage is susceptible to impact injury, occurring either naturally such as in accidents, or iatrogenically during certain surgical procedures such as osteochondral graft insertion. Such injury may progress to posttraumatic arthritis due to limited healing potential of the cartilage [1, 2]. Understanding the mechanobiological factors that cause damage to the cartilage may facilitate early intervention to improve cartilage survival. Previous studies have used isolated osteochondral samples (OCS) to assess impact mechanics and consequent injury to articular cartilage. Two features of cartilage damage are fissure formation [3-5] and chondrocyte death [3, 6-8]. When there is more fissure formation, chondrocyte death tends to aggregate along the surface fissure lines; otherwise, cell death occurs in a more diffuse pattern [3, 5].

Various mechanical factors during impact have been suggested to cause cartilage damage. Chondrocyte death is associated with impact force [9-11], contact stress [3, 7], compressive stress rate [5, 12], compressive strain [3, 13], compressive strain rate [14], and total impact energy [8, 15, 16] applied to adult bovine osteochondral cylinders. Studies of OCS insertion for osteochondral defect repair, either using human cadaveric [10, 17], animal *in vivo* [18] or *in vitro* [11, 19] models, assessed applied energy, the resultant force and impulse, and number of impaction taps required for insertion. However, the exact mechanical stimuli causing such damage are unknown.

Impact energy delivered to biological tissue can transform into border free surface energy creating cracks. Fracture mechanics theory states that crack propagation occurs when energy delivered to the material overcomes the resistance of the material [20]. Such an energy criterion approach has been used to quantify the severity of articular fractures after normalizing such energy to interfragmentary bone surface area [21, 22]. Similarly, articular cartilage damage during impact may be associated with impact energy density, either normalized to total cartilage volume [15, 16] or contact articular cartilage surface area [23, 24].

In certain scenarios, part of the impact energy can be absorbed by other components in the system. For example, in traumatic events such as traffic accidents or sports injury, there may be soft tissue interposition, or concomitant muscle reaction that counteracts the applied load or dissipates the traumatic energy. During osteochondral graft insertion to repair cartilage defect, certain surgical instrument designs incorporate impact load dispensing or absorbing material in the route of graft delivery to reduce injury to the cartilage of the graft [25]. To address these practical scenarios, a cushioning mechanism in the impact testing system can provide a good analog to such energy partitioning and therefore facilitate the study of the mechanics and the resultant biological responses. The hypothesis that energy density delivered to the osteochondral sample is a critical biomechanical determinant of impact injury to articular cartilage. The objectives of the present study were: (1) to determine the effect of applied energy level and cushioning on impact mechanics and articular cartilage damage, (2) to correlate articular cartilage damage with mechanical variables.

2.3 Materials and Methods

Study Design

In the following study, a number of biomechanical variables (**Table 2.1**) associated with osteochondral sample impact were quantified, based on axial load, $F(t)$, and displacement, $u^{AC,OCS}(t)$, measurements as well as optical visualization of the sample during the impact event. Biological damage to articular cartilage was assessed as total crack length (L_{crack}) and viability of chondrocytes at the cartilage surface ($V^{AC,OCS}$).

During OCS Impact, the effects of total applied energy density and cushioning on mechanical variables as well as damage to the OCS articular cartilage were analyzed with four study groups, each with n=6 samples: (1) ϱ^{PE} =7.6 mJ/mm^2, without cushioning, (2) ϱ^{PE} =7.6 mJ/mm^2 with cushioning, (3) ϱ^{PE} =22.9 mJ/mm^2, without cushioning, or (4) ϱ^{PE} =22.9 mJ/mm^2, with cushioning. The two levels of ϱ^{PE} were chosen based on pilot studies to cause mild and severe cartilage damage, respectively. The structural stiffness of the cushion was 190 N/mm, similar to the stiffness of the OCS under the impact conditions of this study, with the expectation of diverting approximately half of the applied energy from the OCS to the cushion.

Cushion Material

The cushioning was provided with a round shaped silicon rubber material of diameter 12.0 mm and thickness (h^{CU}) 3.3 mm, with 40 Durometer.

OCS Preparation

A total of 24 OCS, 2.4 mm in radius ($a^{SCB,OCS}$) with 5.0 mm subchondral bone height ($h^{SCB,OCS}$), were prepared from the knees of adult bovines within 24h of sacrifice, essentially as described previously [26]. Adult bovine tissue was obtained from an abattoir. The distal parts of four femora were isolated from four animals. Each OCS was harvested using a custom made hardened steel coring bit. Continuous irrigation was performed throughout the harvesting procedure with phosphate-buffered saline (PBS) solution supplemented with antibiotics and antimycotics (100 U/mL penicillin, 100 mg/mL streptomycin, and 0.25 mg/mL amphotericin B, PSF) to minimize thermal damage. The edge of the articular cartilage of the OCSs was trimmed using a 3.0 mm sterile dermal punch (Integra Miltex, York, PA), leaving a center pin of cartilage 1.5 mm radius ($a^{AC,OCS}$) and articular surface area ($A^{AC,OCS}(t_{0-})$) of 7.07 mm^2.

Impact Loading and Data Acquisition

A drop tower, validated to assess impact biomechanics, combining some features of previous designs [4, 27, 28] was used to apply impact load with known potential energy to the OCSs and obtain measures of biomechanical variables (**Figure 2.1**). Impact was delivered through a customized rigid stainless steel surgical tamp (weight = 50 g) with flat surfaces (area=113 mm^2) at both ends, with in-line mechanical load cell and tamp displacement sensor. The tamp was in direct contact with the articular surface of the OCSs. The cushion described above can be optionally included in-line between the load cell and the rigid tamp.

The load signals were obtained using a load cell (PCB208C05, PCB Piezotronics, Depew, NY) with 10 kHz sampling rate. The displacement was obtained using a laser displacement sensor (Acuity AR200, Schmitt Industries, Portland, OR) with 1 kHz sampling rate. Total applied energy density, ϱ^{PE}, was computed as potential energy of the drop mass normalized to $A^{AC,OCS}(t_{0-})$.

Cartilage Thickness Measurement

Cartilage thickness before ($h^{AC,OCS}(t_{0-})$) and after impact ($h^{AC,OCS}(t_{24hr+})$) were determined by imaging the samples from the side, perpendicular to the long axis of the sample, with a scale bar under reflected light microscopy. The images were taken from four views with 90 degrees rotation around the long axis to each other. The distance from the center of cartilage-bone junction to the center of surface of cartilage was measured in pixels then converted to the unit of mm according to the scale bar, using NIH ImageJ software. Cartilage thickness was quantified by averaging the values obtained from the four views.

Mechanical Data Analysis

Quantification of mechanical variables was based on measurements of contact force and the concomitant displacement as functions of time throughout the impact event. Both load and displacement data underwent moving average of 1 ms data acquisition time. Relative zero for both force and displacement data was defined as the averaged value of 2 ms of data prior to releasing the drop mass. Contact force ($F(t)$) was determined by subtract relative zero from the load data. Relative zero for time (t_0) was defined as the time point where $F(t_0) > 0.5$ N. Peak contact force (F_p) occurred at

the time point t_{Fp}. Peak contact stress (σ_p) was calculated by normalizing F_p to $A^{AC,OCS}(t_{0-})$. The duration of the loading (T) was determined as the time interval between half peak force ($\frac{1}{2}F_p$) before and after F_p. The impulse (I_c) of the impact event was then calculated by integrating $F(t)$ over the time range encompassing T (**Figure 2.2A**).

Axial compressive displacement of articular cartilage of OCS ($u^{AC,OCS}(t)$) was determined by subtract relative zero from the displacement data. The quantification of axial displacement of the cartilage ($u^{AC,OCS}(t)$) based on measurement of the compression of the OCS under the rigid tamp. This included the compression of both the cartilage and the subchondral bone. The compressive modulus of adult bovine subchondral bone can be as high as 10 GPa [29] and that of the articular cartilage ranges from 0.3 to 49 MPa depending on the loading condition [30-32]. The average cartilage thickness ($h^{AC,OCS}(t_{0-})$) and subchondral bone height ($h^{SCB,OCS}$) were 1.5 and 5.0 mm, and the cross sectional area of the cartilage and bone were 7.07 and 18.10 mm^2, respectively. Accordingly, the ratio of structural stiffness of [cushion : cartilage : bone] was approximately [1:1:191]. Based on the assumptive model of three elastic materials connected in serial and therefore sustaining the same loading force, law of mechanics indicates the compressive displacement ratio, and consequently the energy delivery ratio of [cushion : cartilage : bone] to be as such. We therefore considered $h^{SCB,OCS}$, and subsequently the radius of the subchondral bone ($a^{SCB,OCS}$), were constant throughout the impact event.

Peak axial displacement ($u_p^{AC,OCS}$) occurred at time point t_{up}. Peak axial strain (ε_p) was calculated by normalizing $u_p^{AC,OCS}$ to $h^{AC,OCS}(t_{0-})$ (**Figure 2.2B**). The energy delivered to the sample (W^{OCS}) was calculated by integrating $F(t)$ over $u^{AC,OCS}(t)$ from zero to $u_p^{AC,OCS}$, then normalized to $A^{AC,OCS}(t_{0-})$ to obtain the energy density delivered to the sample (ϱ^{OCS}). The fraction of energy density delivered to the sample was therefore $\varrho^{OCS}/\varrho^{PE}$. The dissipated energy ($W_{DS}{}^{OCS}$) was calculated by integrating the closed area inside the force-displacement hysteresis loop, then normalizing such value to $A^{AC,OCS}(t_{0-})$ to obtain dissipated energy density ($\varrho_{DS}{}^{OCS}$) (**Figure 2.2C**).

Subsequent to impaction, the drop mass was left on the tamp to generate a static load (F_s) for 0.5 s then lifted off to unload the tamp. The total time duration of data acquisition was 2 s.

Cartilage Damage Assessment

Matrix damage was assessed by quantifying the overall length of cracks (L_{crack}) on articular cartilage surface one day after impact. Samples were stained using India Ink essentially as described previously [33, 34]. Surface image of the articular cartilage of the samples were obtained, together with a scale bar under reflected light microscopy. L_{crack} was determined by half of the measured total length of all edges of cartilage surface cracks, then converted to mm. Articular cartilage surface area post impact ($A^{AC,OCS}(t_{24hr+})$) were measured using area selection tool then converted to mm^2. Image processing and measurements were done using NIH ImageJ software.

Surface chondrocyte viability ($V^{AC,OCS}$) was defined as (live cells) / (live + dead cells) in the 2.7×0.75 mm^2 central area across the diameter of the articular cartilage

surface. Samples were incubated for 24hr in tissue culture medium [35], stained with LIVE/DEAD® then imaged *en face* using fluorescence microscopy, essentially as described previously [17, 36]. Only some of the samples underwent chondrocyte viability assessment (four, two, three, two samples for group 1, 2, 3, 4, respectively).

Statistics

The effects of ϱ^{PE} and cushioning on $A^{AC,OCS}(t_{24h+})$, F_p, F_s, $h^{AC,OCS}(t_{0-})$, $h^{AC,OCS}(t_{24h+})$, I_c, L_{crack}, T, t_{Fp}, t_{up}, $u_p^{AC,OCS}$, $u_s^{AC,OCS}$, $V^{AC,OCS}$, W_{DS}^{OCS}, W^{OCS}, ε_p, ϱ_{DS}^{OCS}, ϱ^{OCS}, $\varrho^{OCS}/\varrho^{PE}$, σ_p were assessed by two-way ANOVA. The relationship between total crack length and each of the mechanical variables was assessed by linear regression. Data are expressed as mean±SD. $V^{AC,OCS}$ and ε_p were arcsine-transformed and the other data were log-transformed before statistical analysis. Significance was set at α=0.05.

2.4 Results

Cushioning and the magnitude of ϱ^{PE} both had effect on impact mechanics (**Table 2**). Higher ϱ^{PE} resulted in higher *F(t)* and therefore higher σ_p, while cushioning resulted in lower *F(t)* and σ_p. *T* was longer in samples loaded with cushioning as well as with lower ϱ^{PE}. Higher ϱ^{PE} and cushioning both resulted in higher I_c (**Figure 2.3A**).

Higher ϱ^{PE} resulted in higher $u_p^{AC,OCS}$ and ε_p, while cushioning resulted in lower $u_p^{AC,OCS}$ and ε_p (**Figure 2.3B**). Both W^{OCS} and W_{DS}^{OCS}, and therefore ϱ^{OCS} and ϱ_{DS}^{OCS}, were higher in samples loaded with higher ϱ^{PE} and without cushioning (**Figure 2.3C**). $\varrho^{OCS}/\varrho^{PE}$ did not vary with ϱ^{PE}, but decreased to around 50% with cushioning.

The resultant mean value of L_{crack} was about three times higher in samples loaded with higher ϱ^{PE} compared to lower ϱ^{PE}, and decreased 50% and 83% with cushioning, respectively (**Figure 2.3D-E**). There was no interactive effect between ϱ^{PE} and cushioning on any of the above variables.

Higher ϱ^{PE} resulted in a shorter t_{Fp} and cushioning resulted in longer t_{Fp} (**Figure 2.3A**), without interaction. t_{up} did not vary with ϱ^{PE} or cushioning (**Figure 2.3B**), but there was interactive effect. t_{Fp} occurred prior to t_{up}, except for samples loaded with lower ϱ^{PE} with cushioning.

ϱ^{OCS} was the mechanical variable most closely correlated with the extent of cartilage damage. L_{crack} was strongly correlated with ϱ^{OCS} (R^2=0.91, **Figure 2.4A**), σ_p (R^2=0.88. **Figure 2.4B**) as well as ϱ_{DS}^{OCS} (R^2=0.89), moderately correlated with ε_p (R^2=0.53, **Figure 2.4C**) and *T* (R^2=0.45, **Figure 2.4D**) (each $p<0.001$). L_{crack} was

weakly correlated with $\varrho^{OCS}/\varrho^{PE}$ (R^2=0.31, **Figure 2.4E**, p<0.01), but not correlated with I_c (R^2=0.19, **Figure 2.4F**, p<0.05).

Chondrocyte death was evident adjacent to cracks, or else in a more diffuse pattern in the absence of cracks (**Figure 2.3F-G**). Cushioning had protective effect on $V^{AC,OCS}$, with the highest mean value of 88% in samples loaded with lower ϱ^{PE} with cushioning, where there was minimal L_{crack} present. The grand mean of cartilage thickness before impact, $h^{AC,OCS}(t_{0-})$ was 1.54 mm and did not differ among the four study groups, and increased slightly 24 hours after impact. $A^{AC,OCS}(t_{24hr+})$ was larger with higher ϱ^{PE} and smaller with cushioning, but there was interactive effect.

2.5 Discussion

The impact event was therefore illustrated with more articular cartilage tissue deformation for samples loaded without cushioning (**Figure 2.5A**). Inclusion of the cushion partitioned part of the impact energy and resulted in less resultant $u_p^{AC,OCS}$ and thus less cartilage deformation (**Figure 2.5B**).

The results described here indicated that damage to the articular cartilage, in the form of surface cracks formation in OCS impact was most strongly correlated with energy density delivered to the sample, ϱ^{OCS}, as well as the dissipated energy density ϱ_{DS}^{OCS}. Increased ϱ^{OCS} led to more tissue damage represented by articular cartilage cracks and cell death adjacent to the crack lines. ϱ^{OCS} was determined by the spatiotemporal behavior of the articular cartilage under load, namely by the integration of force on displacement as functions of time encompassing the impact event, including both stored and dissipated energies. The experimental settings combining two levels of applied energy density and the optional cushion material resulted in a range of ϱ^{OCS} linearly correlated to the total crack length, L_{crack}, suggesting that energy density delivered to the sample may be the critical biomechanical determinant of material damage to articular cartilage.

The analysis of energy density and assessment of articular damage require some remarks on certain theoretical and experimental issues. The determination of ϱ^{OCS} was simplified by taking into account only the uniaxial displacement, without considering tissue deformation in other dimensions. *F(t)* was measured on the top of the tamp, which included the friction forces in the impact delivery system. The true

force acting on the OCS during impact may have been less than $F(t)$. The acceleration of the tamp, in addition to that of the drop mass, may have contributed to the resultant $u^{AC,OCS}(t)$ and therefore ϱ^{OCS} as well. Quantification of ϱ^{PE} did not take into account such effect of the tamp. As a result, ϱ^{OCS} may have been overestimated.

The effects of the cushioning on impact biomechanics facilitate study of the biomechanics of osteochondral graft insertion for cartilage defect repair. Cushioning resulted in about 50% decrease of ϱ^{OCS}, which is in accordance with this assumptive model. During the surgical procedure, the applied load advances the graft into the recipient socket. Certain fraction of applied energy transforms to work that moves forward the graft, or at the same time dissipates at the host-graft junction due to friction or tissue deformation. Other part of the applied energy is delivered to the osteochondral graft and can cause damage to the articular cartilage. The partitioning of the applied energy may depend on the insertional tightness of fit. Impact without cushioning approximates the boundary condition of extreme tightness with minimal graft advancement during surgery of OCS insertional repair. In the present study, cushioning decreased about half of the delivered energy fraction to the sample with less resultant damage to articular cartilage. This provides an analog to surgery of OCS insertional repair for cartilage defect, during which the graft advances into the recipient site with less insertional tightness. Cushioning altered the impact mechanics in the way that the contact force and axial compressive displacement both distributed over a wider timeframe with smaller peak value. In addition, this provides information

in future study of the biomechanics of *in vivo* traumatic injury to cartilage with soft tissue interposition.

The pattern of surface chondrocyte death may be explained by distribution of the energy delivered to the sample. In addition to free surface energy of cracks, the energy applied to non-linear, viscoelastic materials also transforms into elastic energy storage as well as viscous, frictional and plastic dissipation. W_{DS}^{OCS} as the energy density inside the hysteresis loop represents the magnitude of energy dissipation during the impact event, and was strongly correlated with L_{crack} in our study. Using modified single edge notch test, the fracture toughness of normal adult canine articular cartilage has been quantified as between 0.14 and 1.50 mJ/mm^2, albeit the test was performed with first creating a notch in the subchondral bone as well as the deep zone of cartilage, then propagate the cracks in the same plane toward the superficial zone [37]. In the present study, the mean value of fracture toughness of cartilage of OCS was 12.0 mJ/mm^2 by normalizing W_{DS}^{OCS} to total crack surface area when assuming that all cracks were full-thickness extending to the cartilage-bone junction. This value is greater than that of the canine model, and lower than that of 36-58 mJ/mm^2 to shear cartilage off the osteochondral junction in adult bovine explants [38]. The difference of cartilage fracture initiation and propagation as well as animal species may also have effect on the measured fracture toughness. In addition, the energy dissipation should be relatively small in regions not adjacent to the cracks [37, 39]. This provides theoretical basis for aggregated cell death along the cracks, which was reported in the literature [3, 5]. When there was no crack of the articular cartilage, energy dissipation

was not shared by creation of cracks, but more evenly distributed across the sample and so was the pattern of cell death. As a result, the effect of ϱ^{PE} on $V^{AC,OCS}$ and the correlation between L_{crack} and $V^{AC,OCS}$ were not obvious in our study.

The present study provided new information of increasing tissue damage with increasing energy density delivered to the sample (ϱ^{OCS}), while the two levels of applied energy density (ϱ^{PE}) were generally in accordance with those reported in the literature. It was suggested that the applied energy density of 1 mJ/mm^3 was the "threshold" of chondrocyte death [3]. Total applied energy density of 30.9 mJ/mm^2 delivered by a metal impactor 5.5 mm in diameter using a drop tower has been described to cause chondrocyte death and cartilage matrix damage of adult bovine osteochondral explants 25 by 25 mm^2 in size [24]. Impact energy delivered by a drop mass, equivalent to applied energy density of 10 to 50 mJ/mm^2 [4] to articular cartilage samples, or 13 and 19 mJ/mm^2 [8] to osteochondral cores have been associated with damage to cartilage. A logarithmic dose-response relationship was found in between applied energy equivalent of 0.9 to 102 mJ/mm^2 and depth of cell death using a spring device on osteochondral cylinders [11]. Since the fraction of delivered energy may vary depending on the boundary conditions of the impact scenario, the energy that is actually delivered to the sample during the impact event (ϱ^{OCS}) may be more critical than total applied energy to the system (ϱ^{PE}).

σ_p was determined by normalizing the peak value of the applied load to contact surface area. However, with the same peak value, how the applied load distributed over such time span of the impact event may elicit different mechanical response in

space and time as well as different biological consequences due to the viscoelasticity of the cartilage tissue. This was shown mechanically in theoretical model [40] and also experimentally using cartilage explants when the tissue was not circumferentially confined [41], and biologically in such unconfined compression setting represented by biosynthetic activity in matrix regulation [41, 42] and cell death [41], as well as in cartilage explants [12], or confined compression of cartilage discs [14]. Therefore, critical stress intensity may be applied to characterize failure behaviors of linear, elastic materials, but less applicable to viscoelastic, inhomogeneous fibrous material such as articular cartilage. Delivered energy density may better represent the impact magnitude sustained by articular cartilage compared to other mechanical factors.

The results provided important information for future modeling of articular cartilage sustaining impact load under a semi-confined condition. In our study, the bottom of the OCS cartilage attaching to the subchondral bone was circumferentially confined, whereas the articular surface is not confined, only with certain degrees of friction at the contact surface with the rigid tamp. The boundary conditions are different from the classic unconfined compression of isolated cartilage samples, or those compressed with a porous platen on the cartilage surface within a circumferentially confining chamber. The volume of the cartilage was relatively conserved during impact type loading [40].

Our study did not assess the direct cause of tissue damage and cell death in cellular level, but our findings brought insights in the biomechanics of articular cartilage damage and mechanobiology of cell death for the above-mentioned

applicable real-life scenarios. This may provide foundations for future work in preserving articular cartilage tissue integrity and chondrocyte survival during surgical procedures such as osteochondral graft insertion for cartilage defect repair.

2.6 Acknowledgments

NIH P01 AG007996 and National Yang-Ming University and Ministry of Education, Taiwan, for fellowship support (AWS).

Chapter 2 has been submitted in full to *Journal of Biomechanics*, Su, Alvin W.; Chen, Yunchan; Dong, Yao; Wailes, Dustin H.; Wong, Van W.; Cai, Shengqiang; Chen, Albert C.; Bugbee, William D.; Sah, Robert L., 2014. The dissertation author was the primary investigator and author of this paper.

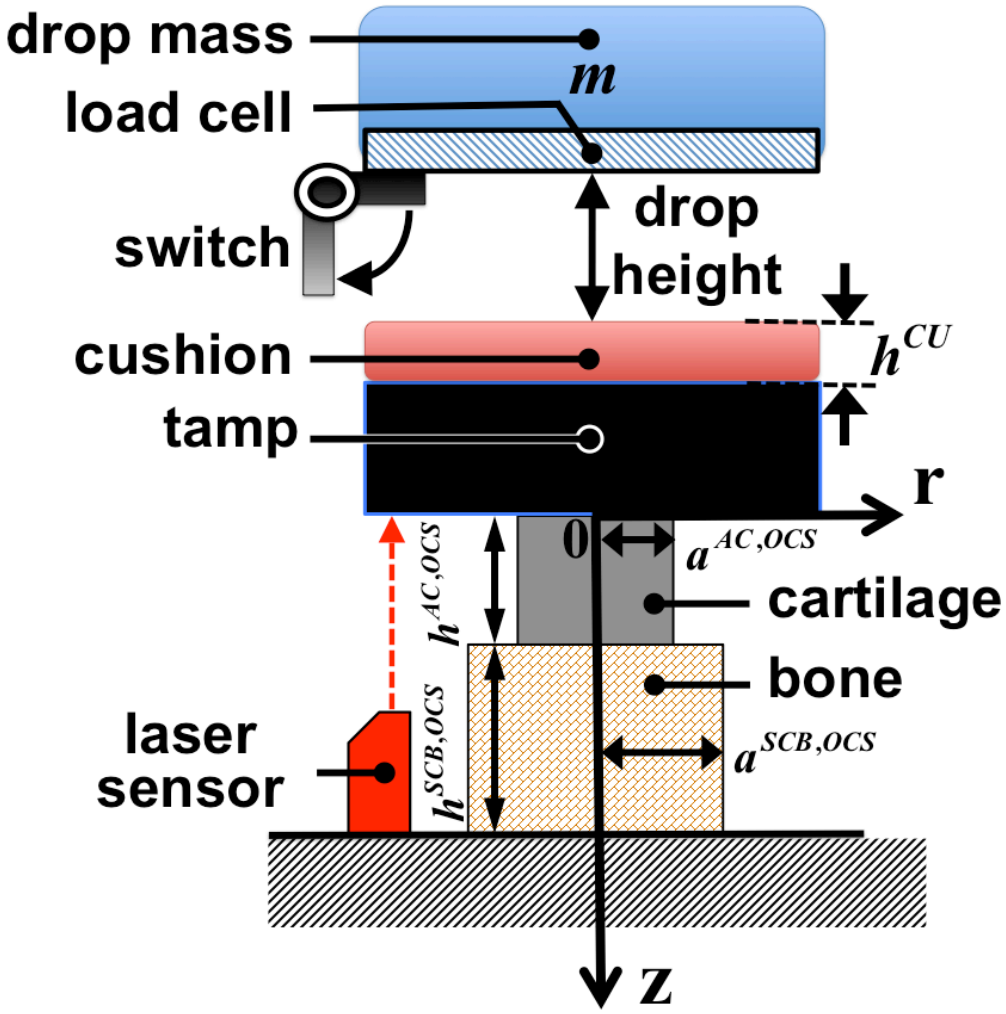

Figure 2.1 Schematic of the drop tower with an optional cushion included in-line between the drop mass and the rigid tamp**.**

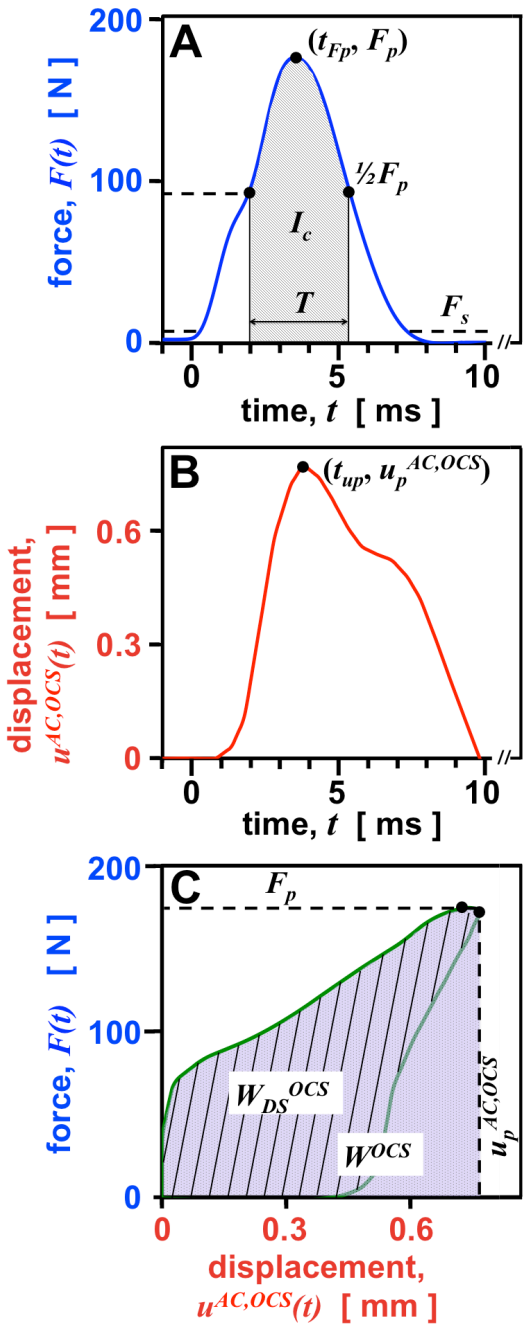

Figure 2.2 Definition and quantification of mechanical variables based on **(A)** force and **(B)** displacement measurements as functions of time, and **(C)** Energy calculation based on force as a function of displacement.

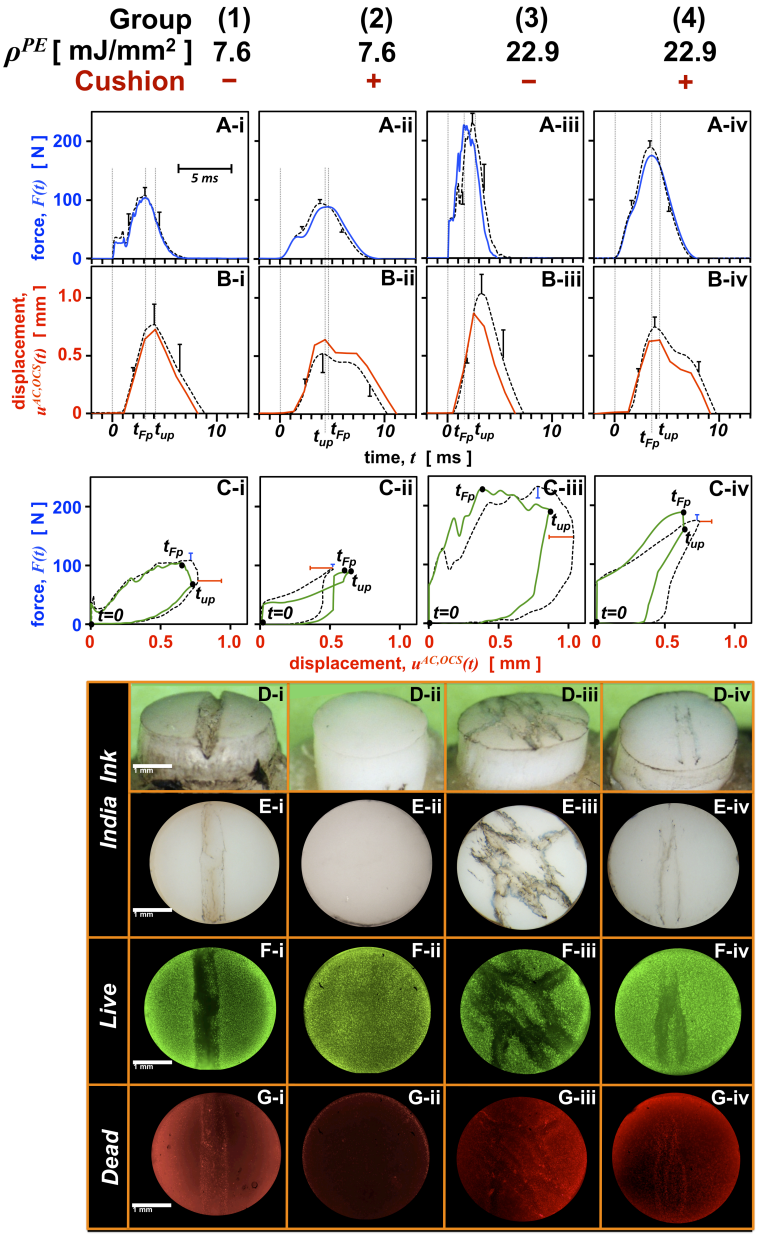

Figure 2.3 Effect of applied energy density (ρ^{PE}) and cushioning on impact mechanics and biological outcomes. **(A)** force, **(B)** displacement, **(C)** energy loop. Articular cartilage of samples were stained with India Ink to visualize surface cracks from **(D)** oblique, and **(E)** *En Face* views. Chondrocyte viability was determined under fluorescence microscopy to visualize **(F)** live cells in green, and **(G)** dead cells in red. Roman number **(i-iv)** represent the four study groups. In **(A-C)**, solid colored lines represent typical sample in the group, and black dashed lines represent group mean±SD (n=6 each)

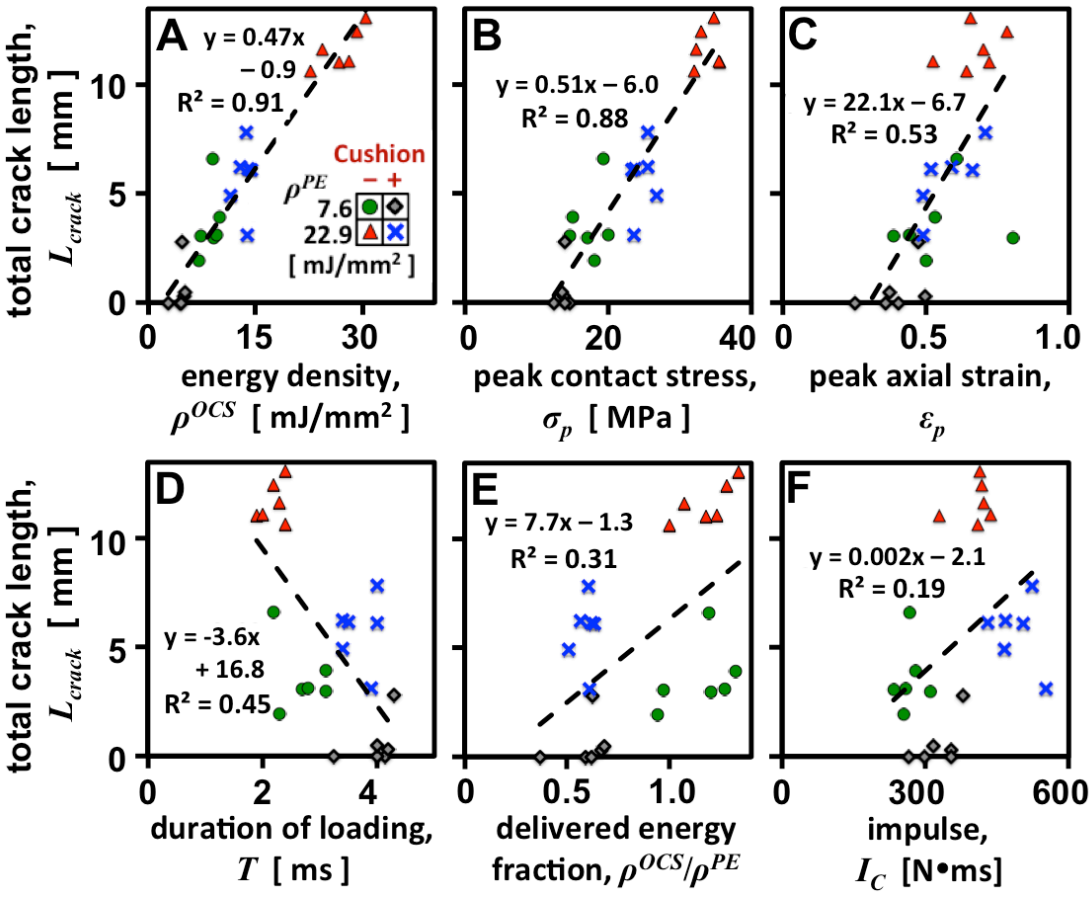

Figure 2.4 Correlation analysis of articular cartilage damage with mechanical variables.

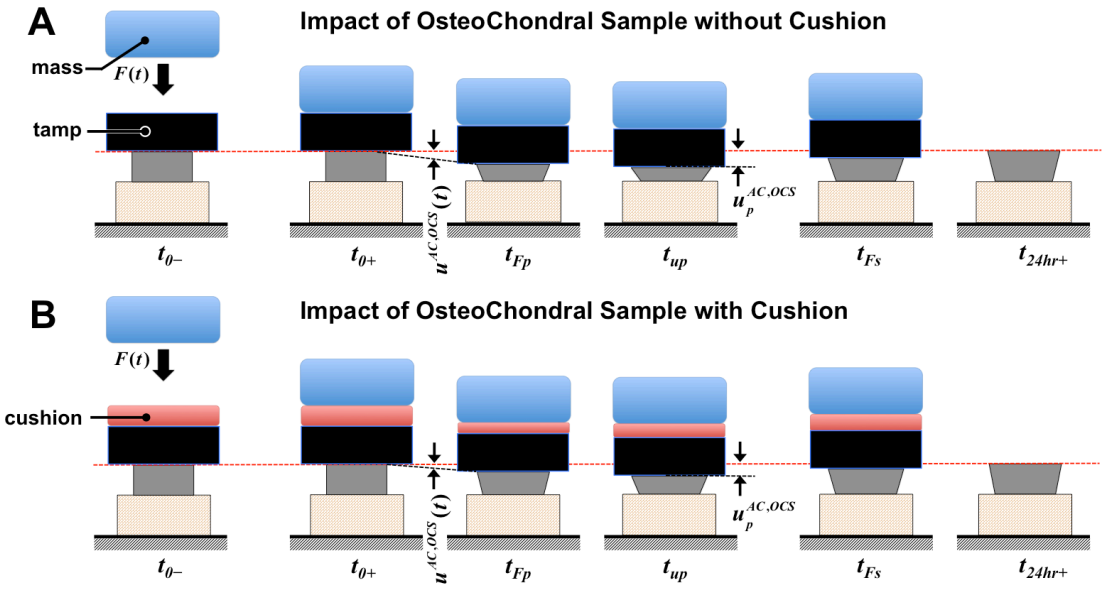

t	t_{0-}	t_{0+}	t_{Fp}	t_{up}	t_{Fs}
$F(t)$	0	> 0	F_p	$< F_p$	F_s
$u^{AC,OCS}(t)$	0	0	$< u_p^{AC,OCS}$	$u_p^{AC,OCS}$	$u_s^{AC,OCS}$
Critical Event	prior to loading	impact load on OCS begins	peak contact force occurs	peak cartilage axial compression occurs	static load on OCS ends

Figure 2.5 Spatiotemporal schematic of osteochondral sample impact. (A) Without cushion. **(B)** With cushion.

.

Table 2.1 Biomechanical parameters and variables.

parameter	definition	unit
$A^{AC,OCS}(t_{0-})$	articular cartilage surface area prior to impact	mm^2
$a^{AC,OCS}$	radius of AC surface of OCS	mm
a^{OCR}	radius of OCR	mm
$a^{SCB,OCS}$	radius of SCB of OCS	mm
$h^{AC,OCS}(t_{0-})$	thickness of AC of OCS prior to impact	mm
h^{CU}	thickness of the cushion	mm
h^{OCR}	depth of OCR relative to cartilage surface	mm
$h^{SCB,OCS}$	height of SCB of OCS	mm
ϱ^{PE}	total applied energy density during impact	mJ/mm^2

variable	definition	unit
$A^{AC,OCS}(t_{24hr+})$	articular cartilage surface area 24 hours post impact	mm^2
$F(t)$	contact force applied on the tamp	N
F_p	peak contact force applied on the tamp during OCS impact	N
F_s	static load on OCS after impact	N
$h^{AC,OCS}(t_{24hr+})$	thickness of AC of OCS 24 hours post impact	mm
I_c	impact impulse of the OCS impact event	N•ms
L_{crack}	total crack lengths on articular cartilage surface of OCS	mm
T	impact time duration during OCS impact	ms
t	relative timeframe for impact event	ms
t_0	relative zero for time at which impact event begins	ms
t_{Fp}	time at when F_p occurs	ms
t_{up}	time at when u_p occurs	ms
$u^{AC,OCS}(t)$	axial compressive displacement of AC of OCS	mm
$u_p^{AC,OCS}$	peak axial compressive displacement of AC of OCS during OCS insertion or impaction	mm
$u_s^{AC,OCS}$	axial compressive displacement of AC of OCS with static load on OCS	mm
$V^{AC,OCS}$	surface chondrocyte viability of AC of OCS post impact	%
W^{OCS}	energy delivered to OCS	mJ
W_{DS}^{OCS}	dissipated energy	mJ
ε_p	peak axial strain of AC of OCS	mm/mm
ϱ^{OCS}	energy density delivered to OCS	mJ/mm^2
ϱ_{DS}^{OCS}	dissipated energy density	mJ/mm^2
σ_p	peak contact stress	MPa

Table 2.2 The effect of ϱ^{PE} and cushioning on mechanics and biological outcomes. Statistical results are indicated as *** p<0.001, ** p<0.01, * p<0.05, ns: non-significant (with p value), n/a: not applicable.

ϱ^{PE} [mJ/mm^2]	Cushion	$h^{AC,OCS}$ (t_0) [mm]	$h^{AC,OCS}$ (t_{24hr+}) [mm]	$A^{AC,OCS}$ (t_{24hr+}) [mm^2]	F_p [N]	σ_p [MPa]	I_c [N•ms]	T [ms]	t_{Fp} [ms]	t_{up} [ms]	$u_p^{AC,OCS}$ [mm]	ε_p	W^{OCS} [mJ]	$W_{DS}{}^{OCS}$ [mJ]	ϱ^{OCS} [mJ/mm^2]	$\varrho_{DS}{}^{OCS}$ [mJ/mm^2]	ϱ^{OCS} / ϱ^{PE}	L_{crack} [mm]	$V^{AC,OCS}$ [%]
7.6	–	1.59 ±0.18	1.65 ±0.19	7.88 ±0.64	123 ±15	17.4 ±2.2	267 ±26	2.7 ±0.4	3.1 ±0.6	3.9 ±0.6	0.86 ±0.20	0.55 ±0.15	62 ±8	49 ±7	8.7 ±1.2	7.0 ±0.9	1.15 ±0.16	3.6 ±1.6	79 ±15
7.6	+	1.58 ±0.26	1.62 ±0.10	7.18 ±0.36	97 ±5	13.8 ±0.7	328 ±42	4.0 ±0.4	4.1 ±0.5	3.7 ±0.7	0.61 ±0.08	0.39 ±0.09	32 ±6	20 ±2	4.5 ±0.9	2.9 ±0.3	0.59 ±0.11	0.6 ±1.1	88 ±15
22.9	–	1.63 ±0.31	1.69 ±0.35	10.92 ±1.51	240 ±12	33.9 ±1.6	405 ±38	2.2 ±0.2	2.2 ±0.4	3.1 ±0.5	1.08 ±0.20	0.67 ±0.09	190 ±21	169 ±20	26.9 ±2.9	23.9 ±2.9	1.18 ±0.13	11.4 ±0.7	72 ±25
22.9	+	1.37 ±0.22	1.44 ±0.19	8.28 ±0.74	175 ±10	24.8 ±1.4	490 ±44	3.7 ±0.3	3.5 ±0.1	4.0 ±0.3	0.78 ±0.10	0.58 ±0.09	95 ±7	67 ±7	13.4 ±1.1	9.4 ±1.0	0.59 ±0.05	5.7 ±1.6	75 ±8
Effect of ϱ^{PE} (p-value)		0.33	0.31	***	***	***	***	**	***	0.33	**	**	***	***	***	***	0.76	***	0.12
Effect of cushioning (p-value)		0.18	0.14	***	***	***	***	***	**	0.13	***	*	***	***	***	***	***	***	*
Interactive effect (p-value)		0.23	0.31	*	0.20	0.20	0.94	0.16	0.13	*	0.84	0.58	0.70	0.57	0.70	0.57	0.76	0.06	0.30
L_{crack} regression, (R^2)		n/a	n/a	n/a	0.88 ***	0.88 ***	0.19 *	0.45 ***	n/a	n/a	0.54 ***	0.53 ***	0.91 ***	0.89 ***	0.91 ***	0.89 ***	0.31 **	n/a	0.09 (p=0.36)

2.7 References

1. Buckwalter JA, Mankin HJ. Articular cartilage: degeneration and osteoarthritis, repair, regeneration, and transplantation. *Instr Course Lect*. 1998;47:487-504.

2. Buckwalter JA. Articular cartilage injuries. *Clin Orthop Relat Res*. 2002;402:21-37.

3. Repo RU, Finlay JB. Survival of articular cartilage after controlled impact. *J Bone Joint Surg Am*. 1977;59-A:1068-1076.

4. Jeffrey JE, Gregory DW, Aspden RM. Matrix damage and chondrocyte viability following a single impact load on articular cartilage. *Arch Biochem Biophys*. 1995;322:87-96.

5. Ewers BJ, Dvoracek-Driksna D, Orth MW, Haut RC. The extent of matrix damage and chondrocyte death in mechanically traumatized articular cartilage explants depends on rate of loading. *J Orthop Res*. 2001;19:779-784.

6. Loening A, Levenston M, James I, Nuttal M, Hung H, Gowen M, Grodzinsky A, Lark M. Injurious mechanical compression of bovine articular cartilage induces chondrocyte apoptosis. *Arch Biochem Biophys*. 2000;381:205-212.

7. Torzilli PA, Grigiene R, Borrelli J, Jr., Helfet DL. Effect of impact load on articular cartilage: cell metabolism and viability, and matrix water content. *J Biomech Eng*. 1999;121:433-441.

8. Szczodry M, Coyle CH, Kramer SJ, Smolinski P, Chu CR. Progressive chondrocyte death after impact injury indicates a need for chondroprotective therapy. *Am J Sports Med*. 2009;37(12):2318-2322.

9. Kang RW, Friel NA, Williams JM, Cole BJ, Wimmer MA. Effect of impaction sequence on osteochondral graft damage: the role of repeated and varying loads. *Am J Sports Med*. 2010;38(1):105-113.

10. Patil S, Butcher W, D'Lima DD, Steklov N, Bugbee WD, Hoenecke HR. Effect of osteochondral graft insertion forces on chondrocyte viability. *Am J Sports Med*. 2008;36(9):1726-1732.

11. Whiteside RA, Jakob RP, Wyss UP, Mainil-Varlet P. Impact loading of articular cartilage during transplantation of osteochondral autograft. *J Bone Joint Surg Br*. 2005;87:1285-1291.

12. Milentijevic D, Torzilli PA. Influence of stress rate on water loss, matrix deformation and chondrocyte viability in impacted articular cartilage. *J Biomech*. 2005;38:493-502.

13. Torzilli PA, Deng XH, Ramcharan M. Effect of compressive strain on cell viability in statically loaded articular cartilage. *Biomech Model Mechanobiol*. 2006;5(2-3):123-132.

14. Quinn TM, Allen RG, Schalet BJ, Perumbuli P, Hunziker EB. Matrix and cell injury due to sub-impact loading of adult bovine articular cartilage explants: effects of strain rate and peak stress. *J Orthop Res*. 2001;19:242-249.

15. Finlay JB, Repo RU. Energy absorbing ability of articular cartilage during impact. *Med Biol Eng Comput*. 1979 17:397-403.

16. Burgin LV, Aspden RM. Impact testing to determine the mechanical properties of articular cartilage in isolation and on bone. *J Mater Sci Mater Med*. 2008 19:703-711.

17. Borazjani BH, Chen AC, Bae WC, Patil S, Sah RL, Firestein GS, Bugbee WD. Effect of impact on chondrocyte viability during the insertion of human osteochondral grafts. *J Bone Joint Surg Am*. 2006;88:1934-1943.

18. Pallante AL, Chen AC, Ball ST, Amiel D, Masuda K, Sah RL, Bugbee WD. The in vivo performance of osteochondral allografts in the goat is diminished with extended storage and decreased cartilage cellularity. *Am J Sports Med*. 2012;40:1814-1823.

19. Pylawka TK, Wimmer M, Cole BJ, Virdi AS, Williams JM. Impaction affects cell viability in osteochondral tissues during transplantation. *J Knee Surg*. 2007;20:105-110.

20. Anderson TL. *Fracture Mechanics: Fundamentals and Applications*. 2nd ed. Boca Raton, FL: CRC Press; 1995.

21. Beardsley C, Marsh JL, Brown T. Quantifying comminution as a measurement of severity of articular injury. *Clin Orthop Rel Res*. 2004;423:74-78.

22. Beardsley CL, Bertsch CR, Marsh JL, Brown TD. Interfragmentary surface area as an index of comminution energy: proof of concept in a bone fracture surrogate. *J Biomech*. 2002;35(3):331-338.

23. Martin JA, McCabe D, Walter M, Buckwalter JA, McKinley TO. N-acetylcysteine inhibits post-impact chondrocyte death in osteochondral explants. *J Bone Joint Surg Am*. 2009;91:1890-1897.

24. Heiner AD, Smith AD, Goetz JE, Goreham-Voss CM, Judd KT, McKinley TO, Martin JA. Cartilage-on-cartilage versus metal-on-cartilage impact characteristics and responses. *J Orthop Res*. 2013;31:887-893.

25. Frei H, Roder D, Jakob RP, Inventors; Sulzer Orthopedics Ltd., assignee. Instrument, instrument set and a method for the introduction of an osteochondral transplant 2003.

26. Chen AC, Bae WC, Schinagl RM, Sah RL. Depth- and strain-dependent mechanical and electromechanical properties of full-thickness bovine articular cartilage in confined compression. *J Biomech*. 2001;34:1-12.

27. Finlay JB, Repo RU. Instrumentation and procedure for the controlled impact of articular cartilage. *IEEE Trans Biomed Eng*. 1978;25:34-39.

28. Burgin LV, Aspden RM. A drop tower for controlled impact testing of biological tissues. *Med Eng Phys*. . 2007;29:525-530.

29. Rho JY, Ashman RB, Turner CH. Young's modulus of trabecular and cortical bone material: ultrasonic and microtensile measurements. *J Biomech*. 1993;26:111-119.

30. Schinagl RM, Gurskis D, Chen AC, Sah RL. Depth-dependent confined compression modulus of full-thickness bovine articular cartilage. *J Orthop Res*. 1997;15:499-506.

31. Korhonen RK, Laasanen MS, Toyras J, Rieppo J, Hirvonen J, Helminen HJ, Jurvelin JS. Comparison of the equilibrium response of articular cartilage in unconfined compression, confined compression and indentation. *J Biomech*. 2002;35(7):903-909.

32. Park S, Costa KD, Ateshian GA. Microscale frictional response of bovine articular cartilage from atomic force microscopy. *J Biomech*. 2004;37:1679-1687.

33. Chang DG, Iverson EP, Schinagl RM, Sonoda M, Amiel D, Coutts RD, Sah RL. Quantitation and localization of cartilage degeneration following the induction of osteoarthritis in the rabbit knee. *Osteoarthritis Cartilage*. 1997;5:357-372.

34. Temple-Wong MM, Bae WC, Chen MQ, Bugbee WD, Amiel D, Coutts RD, Lotz M, Sah RL. Biomechanical, structural, and biochemical indices of degenerative and osteoarthritic deterioration of adult human articular cartilage of the femoral condyle. *Osteoarthritis Cartilage*. 2009; 17:1469-1476.

35. Pallante AL, Gortz S, Chen AC, Healey RM, Chase DC, Ball ST, Amiel D, Sah RL, Bugbee WD. Treatment of articular cartilage defects in the goat with frozen versus fresh osteochondral allografts: effects on cartilage stiffness, zonal composition, and structure at six months. *J Bone Joint Surg Am*. 2012;94:1984-1995.

36. Pallante AL, Bae WC, Chen AC, Gortz S, Bugbee WD, Sah RL. Chondrocyte viability is higher after prolonged storage at 37 degrees C than at 4 degrees C for osteochondral grafts. *Am J Sports Med*. 2009;37 Suppl 1:24S-32S.

37. Chin-Purcell MV, Lewis JL. Fracture of articular cartilage. *J Biomech Eng*. 1996;118:545-556.

38. Broom ND, Oloyede A, Flachsmann R, Hows M. Dynamic fracture characteristics of the osteochondral junction undergoing shear deformation. *Med Eng Phys*. 1996;18:396-404.

39. Ahsan T, Sah RL. Biomechanics of integrative cartilage repair. *Osteoarthritis Cartilage*. 1999;7:29-40.

40. Armstrong CG, Lai WM, Mow VC. An analysis of the unconfined compression of articular cartilage. *J Biomech Eng*. 1984;106:165-173.

41. Sah RL, Kim YJ, Doong JH, Grodzinsky AJ, Plaas AHK, Sandy JD. Biosynthetic response of cartilage explants to dynamic compression. *J Orthop Res*. 1989;7:619-636.

42. Kim YJ, Sah RL, Grodzinsky AJ, Plaas AH, Sandy JD. Mechanical regulation of cartilage biosynthetic behavior: physical stimuli. *Arch Biochem Biophys*. 1994;311:1-12.

.

.

CHAPTER 3

INSERTION BIOMECHANICS AND CHONDROCYTE VIABILITY OF OSTEOCHONDRAL GRAFTS: EFFECTS OF INTERFERENCE FIT AND MODIFICATION

3.1 Abstract

Osteochondral graft (OCG) repair is one of the most effective surgical treatments for focal articular cartilage defects. Certain amount of impact load was applied to the articular cartilage (AC) of the OCG during surgery and can result in chondrocyte death and matrix damage. The effect of graft-host interference fit (ΔR) on OCG insertion biomechanics and the mechanobiological consequences has not been reported. The hypotheses of the present study were: (a) increasing tightness of graft-host interference fit leads to higher insertion energy and resultant AC damage, and (b) modifying OCG geometry can alter mechanics of impact insertion and therefore reduce insertion energy and resultant AC damage. The insertion biomechanics and graft cartilage were compared among study groups of (1) loose fit (ΔR=0.00mm), (2) moderate fit (ΔR=0.05mm) and (3) tight fit (ΔR=0.10mm), as well as between the same tight fit group and (4) modified OCG (ΔR=0.10mm). Successive taps were

applied to insert OCG into OCR using a drop tower apparatus based on a preset protocol with increasing applied impact energy. Insertion energy (W_{insert}^{Tamp}), energy delivered to AC of OCG ($W_{insert}^{AC,OCG}$), OCG advancement energy (W_{adv}) and other mechanical variables were quantified based on contact force and axial displacement measurements. Cartilage damage was assessed by viability of chondrocytes ($V^{AC,OCG}$) and total crack length (L_{crack}) at surface of AC. Subchondral bone compaction at graft-host interface was assessed qualitatively based on micro-computed tomography (μCT) imaging after insertion. Tighter graft-host fit lead to more total number of taps (N) to complete the insertion, higher W_{insert}^{Tamp}, $W_{insert}^{AC,OCG}$, lower subchondral bone compaction and lower resultant $V^{AC,OCG}$. Under the same tight graft-host fit, Modification of OCG geometry lead to less N, W_{insert}^{Tamp}, $W_{insert}^{AC,OCG}$ and higher resultant $V^{AC,OCG}$, as well as less W_{adv} during the middle portion of insertion. L_{crack} was strongly correlated with $W_{insert}^{AC,OCG}$. The results provided novel and important information for surgical instrument design. Tighter graft-host fit may lead to better graft stability after insertion, with the price of deleterious effect on graft cartilage health. Modification of OCG geometry altered insertion mechanics and may reduce cartilage damage while maintaining mechanical stability and biological integration propensity.

3.2 Introduction

Osteochondral graft (OCG) repair is one of the most effective surgical treatments for focal articular cartilage defects [1, 2]. During insertion, certain amount of impact load was applied to the articular cartilage (AC) of the OCG and may result in chondrocyte death [3]. Viable chondrocytes and cartilage matrix integrity are important for clinical success of the surgery [4, 5].

The biomechanics during the OCG insertion process has not been fully understood. The surgeon applies a total number of taps (N) to insert the OCG into the Osteochondral recipient site (OCR). For each tap #i, The peak force ($F_p[i]$) increases as the OCG advances deeper [6, 7]. $F_p[i]$ increases substantially as the OCG bottoms out [6, 8], and is higher in shorter OCG due to higher structural stiffness [9]. The average time duration of each manually applied tap ($T[i]$) is brief, ranging from 0.5 to 5 ms [3, 5, 7, 8]. However, the distribution of the impact energy delivered to the graft and the resultant tissue strain and OCG advancement has not been reported.

Understanding the mechanobiology of articular cartilage damage is crucial for preserving graft tissue health during surgery. Damage to the AC during OCG impact has been related to various biomechanical factors. Energy density delivered to osteochondral samples was strongly correlated to cartilage matrix damage (**Chapter 2**). Chondrocyte death is associated with $F_p[i]$ during OCG insertion [6, 8], also with impact force [8], contact stress [10, 11], compressive stress rate [12, 13], compressive strain [10, 14], compressive strain rate [15], and total impact energy [16-18] for non-insertional impact scenarios.

The graft-host interference fit (ΔR) between OCG and OCR is one of the key parameters for surgical instrument design. Certain analogous studies have introduced the effect of ΔR on insertion mechanics. The insertional load is higher when driving nails of larger diameter into wood [19]. The interference that exceeds the elastic limits of the inserted and the recipient parts leads to higher resistance to relative motion [20]. Accordingly, tighter fit can be beneficial to graft-host healing due to better post-insertional graft stability, but at the same time can require higher impact energy to complete the insertion. The effect of ΔR on OCG insertion biomechanics and the resultant graft cartilage damage has not been reported.

The hypotheses of the present study were: during OCG insertion into OCR, (a) increasing tightness of graft-host interference fit leads to higher insertion energy and resultant AC damage, and (b) modifying OCG geometry can alter mechanics of impact insertion and therefore reduce insertion energy and resultant AC damage. The specific aims were: to determine the effect of ΔR on (1) biomechanics of OCG insertion, (2) damage to cell and matrix of AC, and (3) to compare the insertion biomechanics and resultant AC damage between standard OCG and modified OCG.

3.3 Materials and Methods

Study Design

Study 1. The effect of ΔR on biomechanics of insertion and damage to articular cartilage was assessed by total energy density delivered to AC of OCG ($W_{insert}^{AC,OCG}$), total tap numbers (N), cumulative OCG advancement distance ($u_{adv}[m]$) as a function of cumulative insertion energy ($W^{Tamp}[m]$) and surface chondrocyte viability ($V^{AC,OCG}$), with three study groups: (1) loose fit: ΔR=0.00 mm (n=7), (2) moderate fit: ΔR=0.05 mm (n=6), (3) tight fit: ΔR=0.10 mm (n=6).

Study 2. The effect of OCG geometry modification on biomechanics of insertion and damage to articular cartilage was assessed with two study groups, both had tight fit, ΔR=0.00 mm: (1) standard OCG (n=6), (2) modified OCG (n=7).

Detailed Experimental Methods

Sample Preparation. A total of 41 OCGs and 26 OCRs were prepared sterilely from distal femora of six adult bovine animals within 24 h of sacrifice, essentially as described before (**Chapter 2**). In short, the radius and subchondral bone height of the OCGs were 2.40 mm and 5.00 mm, respectively. The OCRs were prepared with osteochondral cuboid blocks with around 200 mm^2 base area and 20 mm height. 15 OCGs served as control samples without any impact loading treatment. 19 OCGs were used in *Study 1*. For *Study 2*, Seven OCGs underwent geometry modification, and were compared to the six tight fit samples in *Study 1*.

Graft-host Interference Fit (ΔR) was defined as the radius of the OCG (2.40 mm) minus the radius of the OCR (a^{OCR}). The recipient sites were drilled in the center

of the cuboid blocks to 10 mm of depth from the articular surface to the bottom using stainless steel drill bits of 4.80, 4.70 and 4.60 mm in diameter. Therefore, a^{OCR} was 2.40, 2.35 and 2.30 mm, resulting in three levels of ΔR: 0.00, 0.05 and 0.10 mm (**Fig. 3.1A**).

OCG geometry modification. An offset 2 mm in height and 0.25 mm in depth was created 1.5 mm below the cartilage-bone junction of the OCG (**Fig. 3.1B**). The OCG was mounted on a spinning collet (diameter 4.8 mm) of a drill mill machine, with appropriate protection and hydration of the articular cartilage. A 2.00 mm-thick rectangular hand file was mounted on the platform of the drill mill, and then gently slid inward until 0.25 mm of depth to create the offset.

OCG Insertion. The OCG was pre-inserted manually 1.5 mm into the OCR. Serial taps of impact load ($F(t)$) was then applied to the OCG using the drop tower apparatus essentially as described before (**Chapter 2**). The applied energy density for the first tap (W^{PE}) was 16.0 mJ, and then increased by a factor of 1.5. Thus, for tap #i, $W^{PE} = 16.0 \times 1.5^{(i-1)}$. Serial taps were applied until tap #N (when i=N), after which the articular surface of the OCG was flush with that of the OCR (**Fig. 3.2A**). The articular cartilage of the OCG was sliced off using a sterile scalpel after insertion and incubated 24 h before cell viability analysis, then fixed with PBS + Proteinase Inhibitors, essentially as described before (**Chapter 2**).

Outcome Analysis

The mechanical variables were quantified based on the signals from the load sensor and laser displacement sensor essentially as described before (**Chapter 2**). In short, for each tap, i, peak contact stress ($\sigma_p[i]$) was obtained by normalizing peak

contact force ($F_p[i]$) to the AC surface area of OCG (A^{OCG}, 18.09 mm^2). Impact impulse ($I_C[i]$) was quantified by integrating impact force over the time frame encompassing impact time duration ($T[i]$). Peak axial displacement of AC of OCG ($u_p^{AC,OCG}[i]$) was estimated as peak axial displacement of the tamp ($u_p^{Tamp}[i]$) minus OCG advancement distance during for each tap ($u_{adv}[i]$). Peak axial strain of AC of OCG ($\varepsilon_p[i]$) was obtained by normalizing $u_p^{AC,OCG}[i]$ to thickness of AC of OCG ($h^{AC,OCG}$). For each tap, insertion energy delivered by the tamp to the sample ($W^{Tamp}[i]$) was quantified by integrating $F(t)$ over axial displacement of the tamp ($u^{Tamp}(t)$). Energy delivered to AC of OCG ($W^{AC,OCG}[i]$) and OCG advancement energy ($W_{adv}[i]$) were determined by: (a) $W^{Tamp}[i] \cong W^{AC,OCG}[i] + W_{adv}[i]$, (b) $W^{AC,OCG}[i] : W_{adv}[i] \cong u_p^{AC,OCG}[i] : u_{adv}[i]$ (**Fig. 3.2A**).

Total energy delivered to AC of OCG ($W_{insert}^{AC,OCG}$) was defined as the sum of $W^{AC,OCG}[i]$ of all taps for each OCG. Cumulative OCG advancement distance ($u_{adv}[m]$) and cumulative insertion energy ($W^{Tamp}[m]$) was defined as the sum of $u_{adv}[i]$ and $W^{Tamp}[i]$, from the first tap to tap #m (i=1 to i=m), respectively.

In *Study 2*, data of cumulative OCG advancement energy was interpolated into estimated values (W_{adv}) corresponding to five defined depth of OCG position in OCR, from $u_{adv}[m]$=0.00 to 5.00 mm, each 1.00 mm in depth (**Fig. 3.2B**).

$V^{AC,OCG}$ and L_{crack} were quantified essentially as described before (**Chapter 2**). In short, $V^{AC,OCG}$ was calculated as (live cells) / (live + dead cells) in the 3.75×0.75 mm^2 central area across the diameter of the articular cartilage surface, under fluorescence microscopy 24 hrs after impact insertion of the OCG. L_{crack} was measured after India Ink staining, as the total surface crack length of each OCG, by

three independent observers with repeatable measurement values (intraclass correlation coefficient, ICC=0.98).

Micro-computed tomography (μCT) imaging. Representative sample of each experimental group was chosen for *μCT* scanning for qualitative assessment of the top, middle and bottom parts of graft-host subchondral bone interface, with settings essentially as described before [4]. In short, the samples were scanned at 9 μm^3, and the images were reconstructed using a beam hardening correction algorithm.

Statistical Analysis

The difference of $W_{insert}^{AC,OCG}$, N, $V^{AC,OCG}$ among the four study groups (loose fit, moderate fit, tight fit, tight fit with OCG geometry modification) were assessed using one-way ANOVA. the effect of ΔR on the above variables was then assessed with Tukey post-hoc test. The effect of OCG geometry modification was assessed as planned comparison using two-tailed unpaired student t test.

Study 1. The effects of ΔR on $F_p[i]$, $\sigma_p[i]$, $I_C[i]$, $T[i]$, $u_p^{Tamp}[i]$, $u_p^{AC,OCG}[i]$, $u_{adv}[i]$, $\varepsilon_p[i]$, $W^{Tamp}[i]$, $W^{AC,OCG}[i]$, $W_{adv}[i]$ were assessed using one-way ANOVA for the first five taps ($1 \leq i \leq 5$), and unpaired two-tailed student t test for $6 \leq i \leq 8$.

Study 2. The effect of *OCG geometry modification* on W_{adv} in the five defined insertion depths was assessed using unpaired two-tailed student t test. The effects of *OCG geometry modification* on $F_p[i]$, $\sigma_p[i]$, $I_C[i]$, $T[i]$, $u_p^{Tamp}[i]$, $u_p^{AC,OCG}[i]$, $u_{adv}[i]$, $\varepsilon_p[i]$, $W^{Tamp}[i]$, $W^{AC,OCG}[i]$, $W_{adv}[i]$ were assessed using unpaired two-tailed student t test.

The relationship between L_{crack} and $W_{insert}^{AC,OCG}$ for all OCG samples in both studies was assessed by linear correlation.Data are expressed as mean±SD. Significance was set at $\alpha=0.05$.

3.4 Results

Study 1

Tighter interference fit resulted in more total number of taps and higher total energy delivered to AC of OCG at completion of insertion (**Fig. 3.3A-B**). The tight fit group had two times higher of the mean value of N, and 25 times higher $W_{insert}^{AC,OCG}$ compared to the loose fit group. When looking at $u_{adv}[m]$ as a function of $W^{Tamp}[m]$, tighter interference fit presented a "right-shift" phenomenon of the sigmoid curve (**Fig. 3.3D**). This indicated that more insertion energy was required to reach the same level of OCG advancement into the OCR.

Tighter interference fit led to higher $W^{AC,OCG}[i]$ for the first five taps, higher $W_{adv}[i]$ for the first four taps and higher $F_p[i]$, $\sigma_p[i]$ for the first three taps. Tighter fit led to shorter $T[i]$, $u_p^{Tamp}[i]$ and $u_{adv}[i]$ for tap #3 and #4. $W^{Tamp}[i]$, $u_p^{AC,OCG}[i]$, $I_C[i]$ were generally similar among loose, moderate and tight fit groups except for tap #6. (**Fig. 3.4A-C, Table 2**)

Tighter interference fit resulted in more surface chondrocyte death and cartilage tissue cracks of OCG (**Fig. 3.3C, Fig. 3.4D-F**). The mean value of $V^{AC,OCG}$ was 98%, 94%, 83%, 57% for no load control, loose, moderate and tight fit groups, respectively.

Study 2

Modification of OCG geometry resulted in less total number of taps and lower total energy delivered to AC of OCG at completion of insertion (**Fig. 3.3A-B**). The mean value of N decreased from 9.7 to 7.6, and $W_{insert}^{AC,OCG}$ decreased 72%. When

looking at $u_{adv}[m]$ as a function of $W^{Tamp}[m]$, OCG geometry modification led to a "left-shit" of the sigmoid curve (**Fig. 3.3D**).

Modification of OCG geometry led to lower ${u_p}^{AC,OCG}[i]$, $W^{Tamp}[i]$, ${W}^{AC,OCG}[i]$ and higher $u_{adv}[i]$, $W_{adv}[i]$ at the middle part of insertion (tap #5, #6). The other mechanical variables were generally similar, except for few exceptions (**Fig. 3.4A-C, Table 3**).

Surface chondrocyte death and cartilage tissue cracks were less in modified OCG (**Fig. 3.3C, Fig. 3.4D-F**). The mean value of $V^{AC,OCG}$ was 76% compared to that of 57% of non-modified OCG.

OCG geometry modification resulted in less OCG advancement energy in the middle part of insertion. Modified OCG had lower W_{adv} at defined insertion depth of 1.00 to 4.00 mm, compared to standard OCG (**Fig. 3.5**).

L_{crack} was strongly correlated with ${W_{insert}}^{AC,OCG}$ (R^2=0.93, p<0.0001, **Fig. 3.6**). The mean value of L_{crack} of tight fit group was 11.58 mm, around 100 times higher than that of 0.11 mm of the loose fit group, and almost six times higher than that of 2.04 mm with OCG geometry modification.

Qualitatively, μCT showed that the tight fit sample presented the most apparent subchondral bone compaction at the graft-host interface. Certain thin space was visible at the graft-host interface of the loose fit sample. Such space was less for the moderate fit sample, and least for the tight fit sample. The modified OCG sample exhibited a clearly visible space without subchondral bone contact at the offset middle part of the graft, and pattern similar to the standard OCG at top and bottom of the graft (**Fig. 3.7**).

3.5 Discussion

The present study showed that graft-host interference fit was crucial to OCG insertion biomechanics and the resultant damage to articular cartilage. Tighter fit required more taps and more insertion energy to complete the insertion process and resulted in more cell death. With the same graft-host fit, modification of the subchondral bone geometry altered the biomechanics of insertion and subsequently lessened the damage to the cartilage. These results provided important considerations for surgical instrument design, as increasing graft-host fit may increase graft stability at the price of its potentially deleterious effect on graft cartilage health.

The interpretation of the present study requires some remarks on certain experimental and translational issues. First, adult bovine osteochondral tissue is not identical to that of human in terms of cartilage thickness and material properties. The compressive modulus of adult bovine subchondral bone can be as high as 10 GPa [21] and that of the articular cartilage ranges from 0.3 to 49 MPa depending on the loading condition [22, 23]. The compressive modulus for human subchondral bone and articular cartilage is around 1.15 GPa [24] and 3.1 to 13.0 MPa [25], respectively. In addition, the cartilage height in adult human joints is approximately 2.2 to 2.5 mm [26, 27], compared to the average value of $h^{AC,OCG}$ of 1.50 mm in the present study. Therefore, the biomechanics of insertion can be different when using human tissue, resulting in different mechanobiological consequences to the articular cartilage.

Secondly, the size of OCG and ΔR were on the smaller end of those in clinical practice in order to generate reasonable numbers of samples for statistical purposes.

The diameter of autologous OCG commonly utilized in surgery can be as large as up to 10.0 mm for [1, 28], or even higher for allogenous OCG, and the ΔR ranges from 0.1 to 1.0 mm. In the present study, the diameter of OCGs was 4.8 mm, and the largest ΔR was 0.1 mm. The present study utilized bovine tissue to validate the experimental methodologies to approach the scientific problems of OCG insertion.

In addition, at completion of insertion, a gap was left between the base of OCG and the bottom of the OCR to facilitate biomechanical analysis. Such gap is not commonly seen in clinical practice. The experimental design of the present study focused on the process of graft advancement inside the recipient site. In certain scenarios, impact load is applied when the base of the OCG is in contact with the bottom of the OCR to "bottom out" the graft. This issue was not addressed in the present study. Such situation was shown to be associated with higher insertion load and more cell death [8].

The higher insertion energy for tight fit samples may be explained by the graft-host interface reactions. During each tap, the applied impact energy was partitioned to two major components: the AC of OCG, and the OCG-OCR subchondral bone system. Using the simplified model of two materials connected in serial, law of mechanics indicated that more energy is partitioned into the component with lower equivalent modulus. As the OCG advances further into the OCR, the subchondral bones of both can undergo elastic and plastic deformations, as well as microfracture at the contact surface. The magnitude of the above can increase with increasing graft-host interference fit, thus resulting in a higher equivalent modulus. Therefore, with the same $W^{PE}[i]$, higher ΔR led to higher $W^{AC,OCG}[i]$ and less $u_{adv}[i]$. Consequently, the

tight fit group required more N with higher $W_{insert}^{AC,OCG}$ to complete the insertion, and resulted in more damage to the articular cartilage.

The modification of OCG geometry can decrease the equivalent modulus of the graft-bone subchondral bone system by reducing the graft-host interface contact area. This was shown by the lower W_{adv} in the modified OCG group when the offset part of the OCG subchondral bone advanced into the OCR ($u_{adv}[m]$=1.00 to 4.00 mm). Clinically, the offset space can lead to potentially higher risk of fluid accumulation and subsequent subchondral cyst formation *in vivo*. From the perspective of bone fracture fixation, osseous healing can occur with such space even with certain magnitude of graft-host relative motion [29]. With the same ΔR, the idea of OCG geometry modification may shed light on surgical methods of reducing cartilage damage while maintaining mechanical stability and biological integration propensity.

The effect of ΔR and OCG geometry modification on graft stability after insertion is yet to be elucidated. Graft stability may be associated with graft length and diameter, as well as repeated insertion, by quantifying the pull out load using *ex vivo* porcine model [30]. However, such association should be interpreted with the fact in mind that *in vivo*, the OCG sustains repetitive compressive and shear load after surgery. The results of the present study exhibited that tighter ΔR may provide better resistance of graft movement under compressive impact load. Looser ΔR may be prone to excessive lateral motion because of more space at graft-host junction. The optimal graft-host interference fit can thus rely upon the delicate balance between preserving graft cartilage health and adequate post-insertional graft stability.

In Conclusion, the present study provided new information about the effect of graft-host interference fit on OCG insertion biomechanics and its mechanobiological consequences. Modification of OCG geometry can be an alternative to lessen impact damage to the graft. These findings provided a foundation for additional investigation of related translational problems in the future.

3.6 Acknowledgments

NIH P01 AG007996 and National Yang-Ming University and Ministry of Education, Taiwan, for fellowship support (AWS).

Chapter 3 has been submitted in full to *The American Journal of Sports Medicine*, Su, Alvin W.; Chen, Yunchan; Wailes, Dustin H.; Wong, Van W.; Cai, Shengqiang; Chen, Albert C.; Bugbee, William D.; Sah, Robert L., 2014. The dissertation author was the primary investigator and author of this paper.

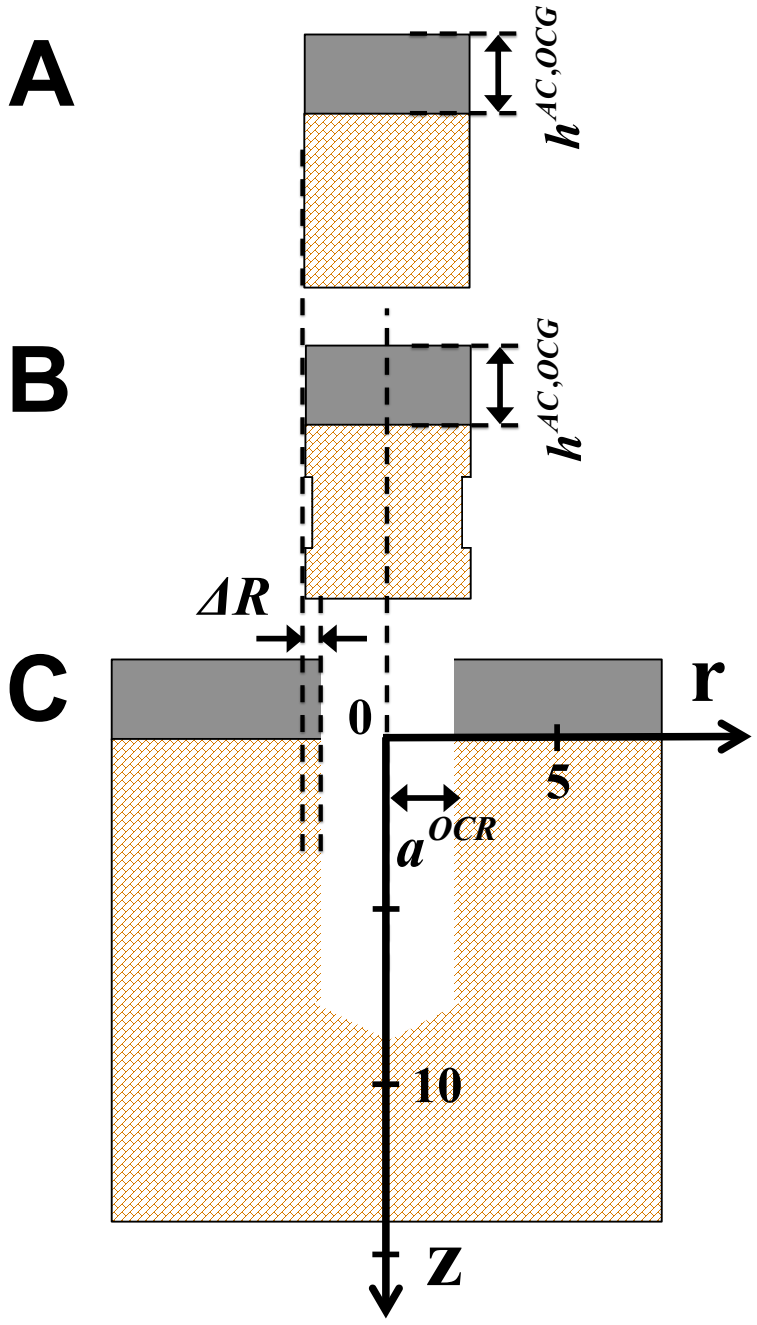

Figure 3.1 Schematic of geometries of OCG and OCR. (A) standard OCG, **(B)** modified OCG, and **(C)** OCR. Indicated is graft-host interference fit (ΔR).

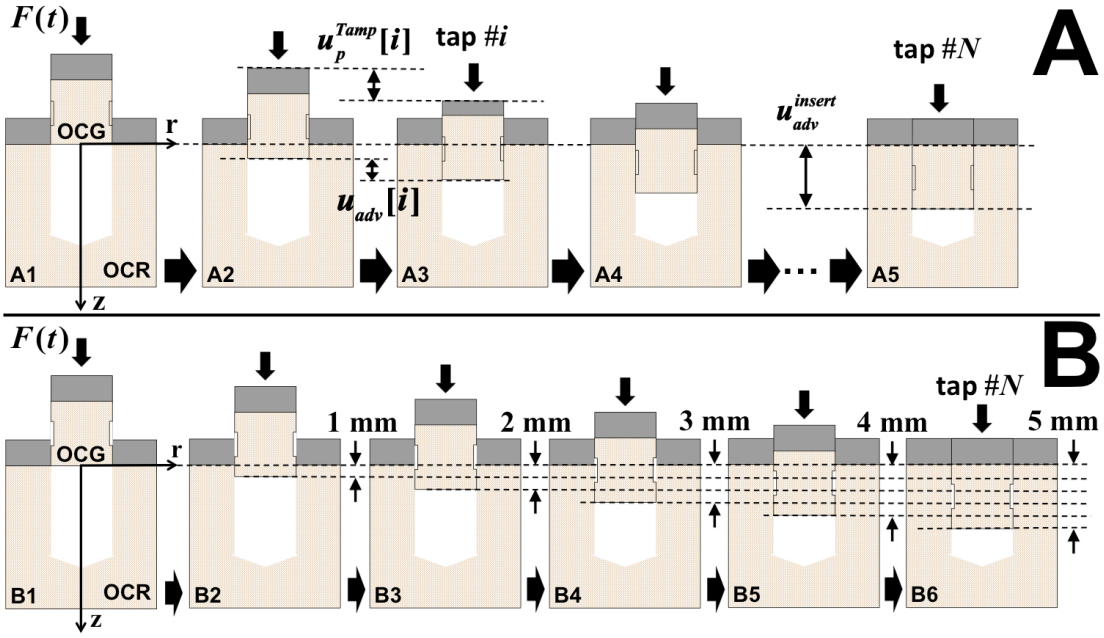

Figure 3.2 Schematic of impact insertion of OCG and mechanical variables and parameters. (A) Advancement of OCG into OCR, starting with flush position (A1), advancing with successive taps (A2-5), to final flush position (A5). Tap #, i, out of N total taps. Tamp advancement with tap i, $u_p^{Tamp}[i]$. OCG (bone base) advancement with tap i, $u_{adv}[i]$, and overall advancement at full insertion, u_{adv}^{insert}. **(B)** OCG at five successive insertion positions, at insertion depths of 1-5 mm (B2-B6), at which parameters were estimated.

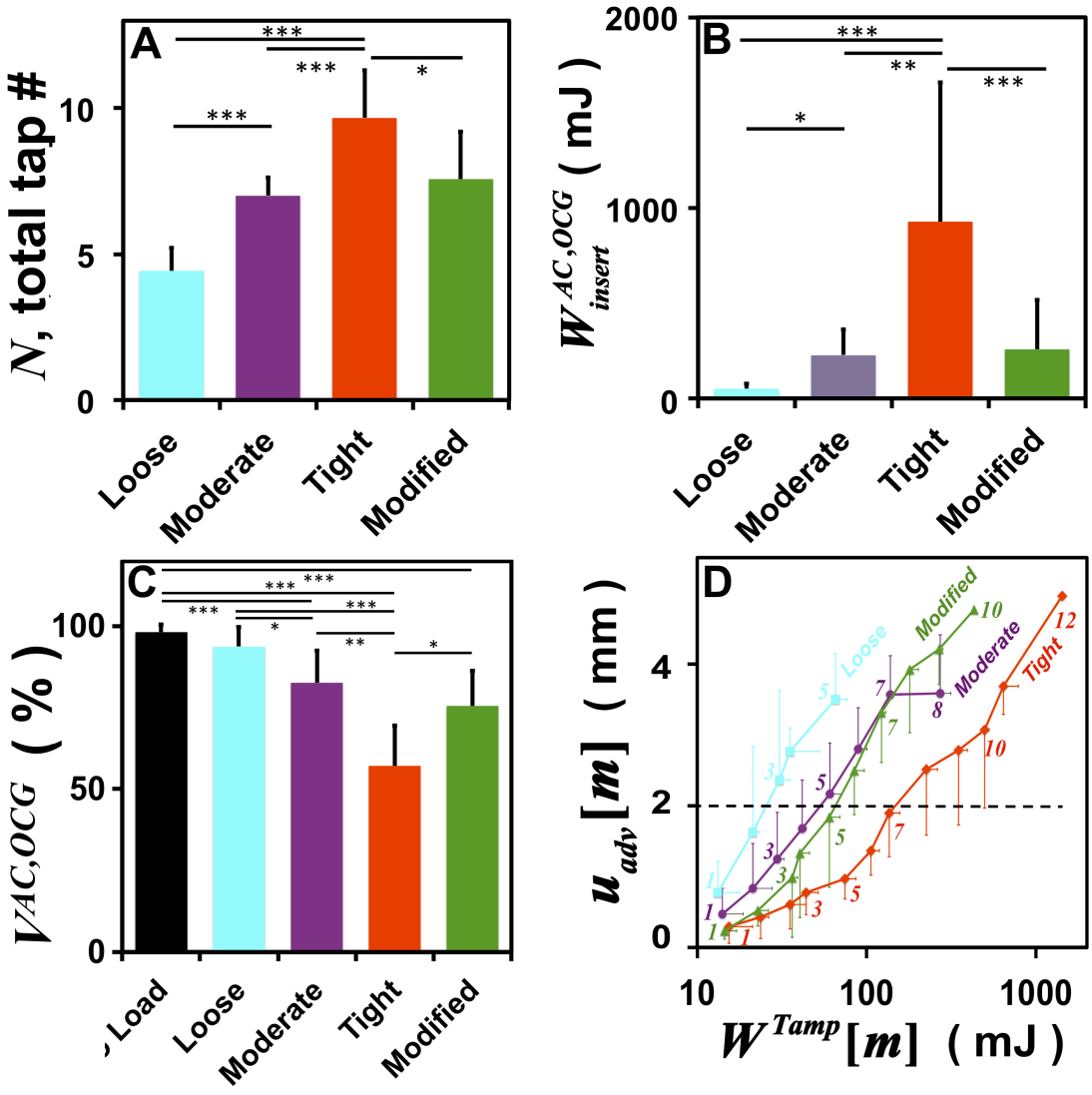

Figure 3.3 Effects of interference fit (ΔR) and OCG geometry modification on insertion mechanics. **(A)** Total number of taps (N). **(B)** Total energy delivered to AC of OCG ($W_{insert}^{AC,OCG}$). **(C)** Viability of surface chondrocytes ($V^{AC,OCG}$). **(D)** Cumulative OCG advancement ($u_{adv}[m]$) as a function of cumulative insertion energy ($W^{Tamp}[m]$), after each tap, i, as labeled.

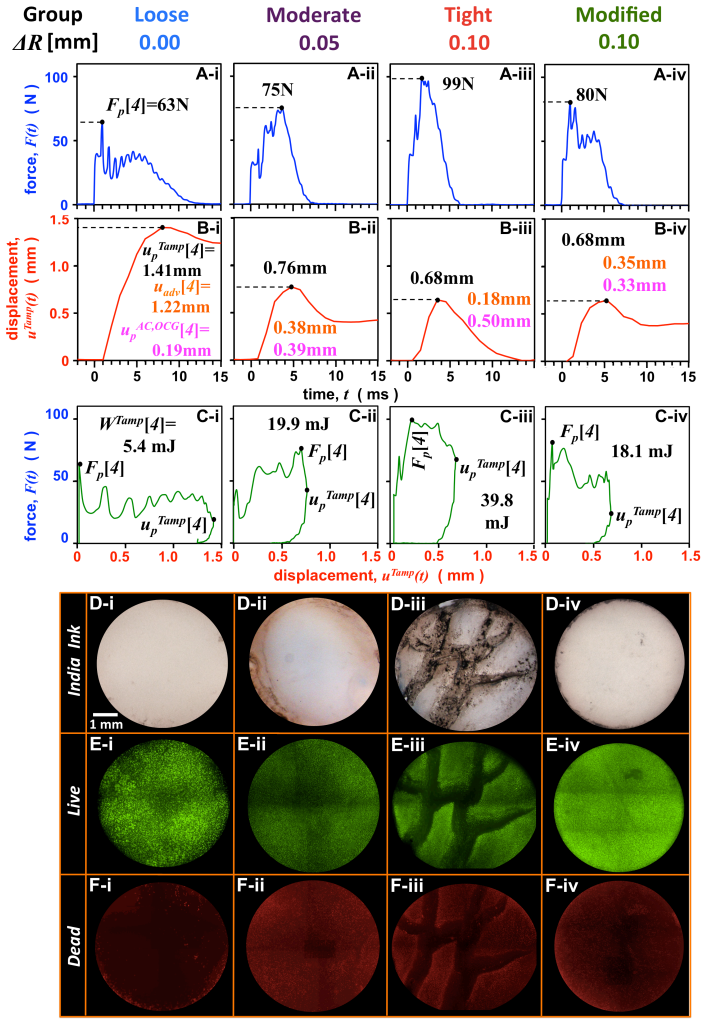

Figure 3.4 Typical effects of interference fit (ΔR) and OCG geometry modification on impact mechanics and cartilage damage. (i-iv) Study Groups are standard OCG geometry with OCR that generate **(i)** loose, **(ii)** moderate, and **(iii)** tight interference fits, and **(iv)** modified OCG geometry into OCR with tight fit. **(A-C)** Mechanics of OCG insertion. For 4th tap, time courses of measured **(A)** tamp contact force, **(B)** tamp displacement and **(C)** parametric plot of tamp contact force and displacement, illustrating energy-associated loop. In **(B)** are indicated peak tamp advancement increment, divided amongst OCG advancement, $u_{adv}[4]$, and deduced cartilage compaction, $u_p^{AC,OCG}[4]$. In **(C)** are indicated delivered energy values. **(D-F)** *En face* microscopic analysis of effects on cartilage. **(D)** Reflected light view of articular surface after India Ink staining, showing cartilage damage and cracks. Fluorescence view of articular surface after Live-Dead fluorescence staining, with **(E)** live cell indicator in green, and **(F)** dead cell indicator in red.

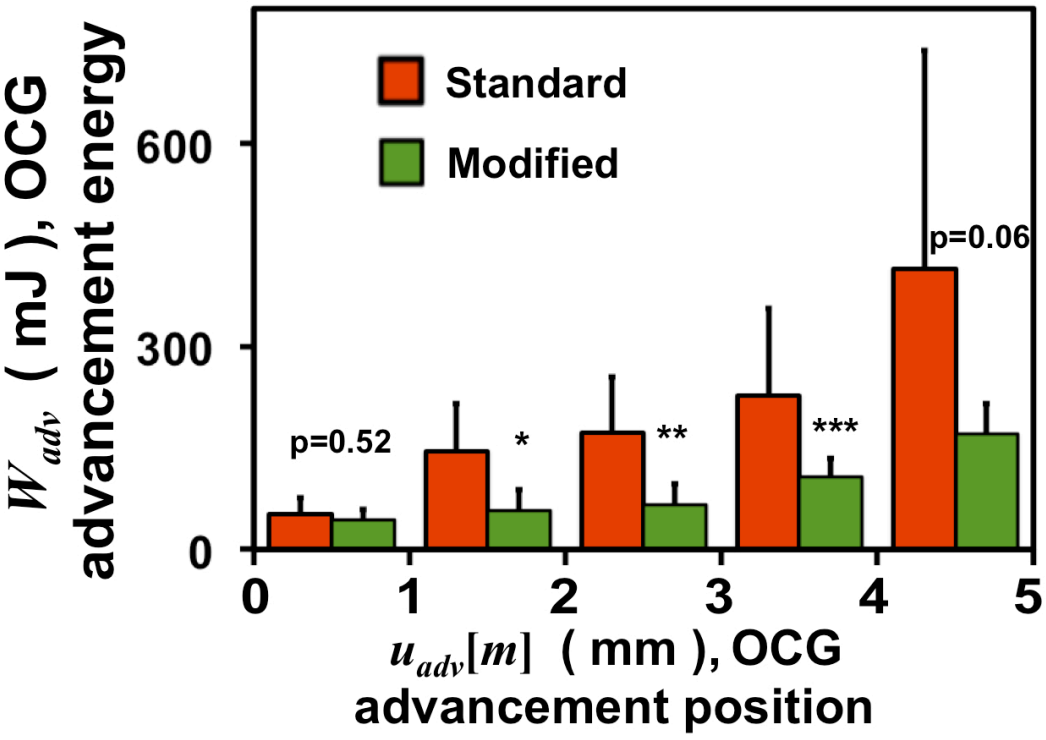

Figure 3.5 Effect of OCG geometry modification on energy for OCG advancement to defined depths. Data of cumulative energy after individual taps was interpolated to estimate values at the indicated positions of 0-5 mm insertion depth.

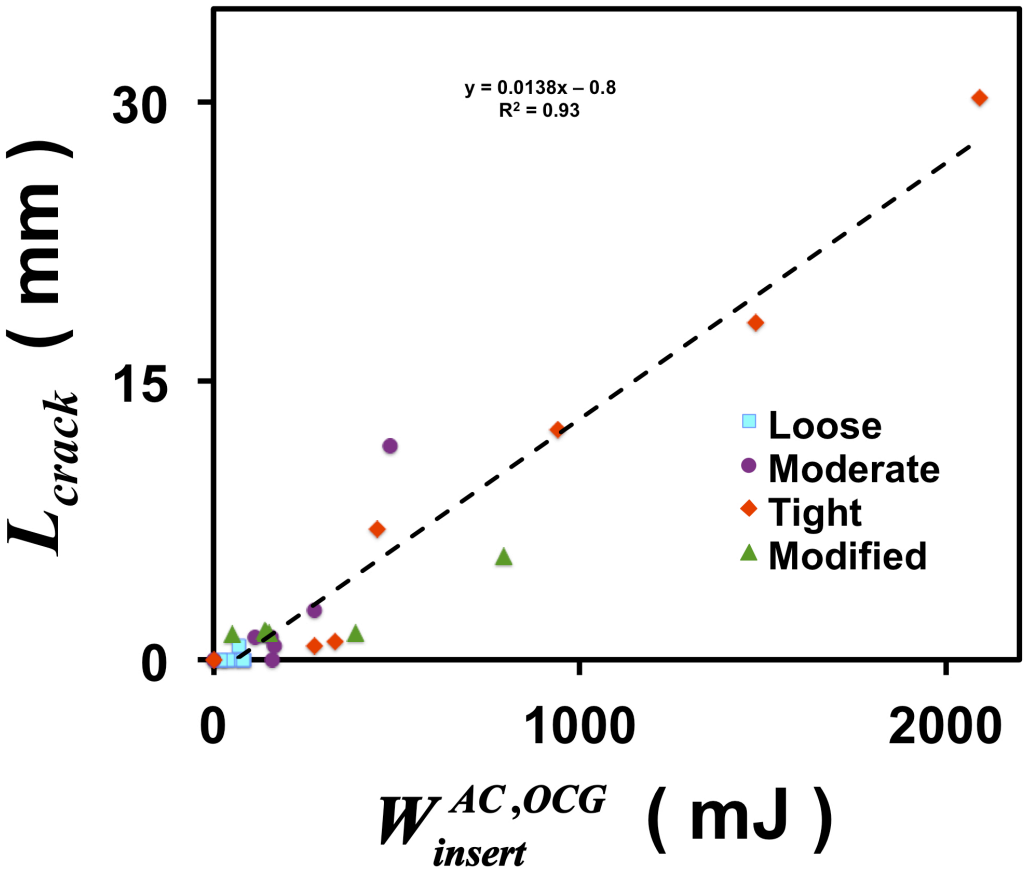

Figure 3.6 Correlation analysis of total crack length on graft cartilage surface (L_{crack}) with total energy delivered to AC of OCG ($W_{insert}^{AC,OCG}$). Data for all samples, with Loose, Moderate, and Tight interference fits of standard samples, and also Tight interference fit of modified samples are indicated with colored symbols.

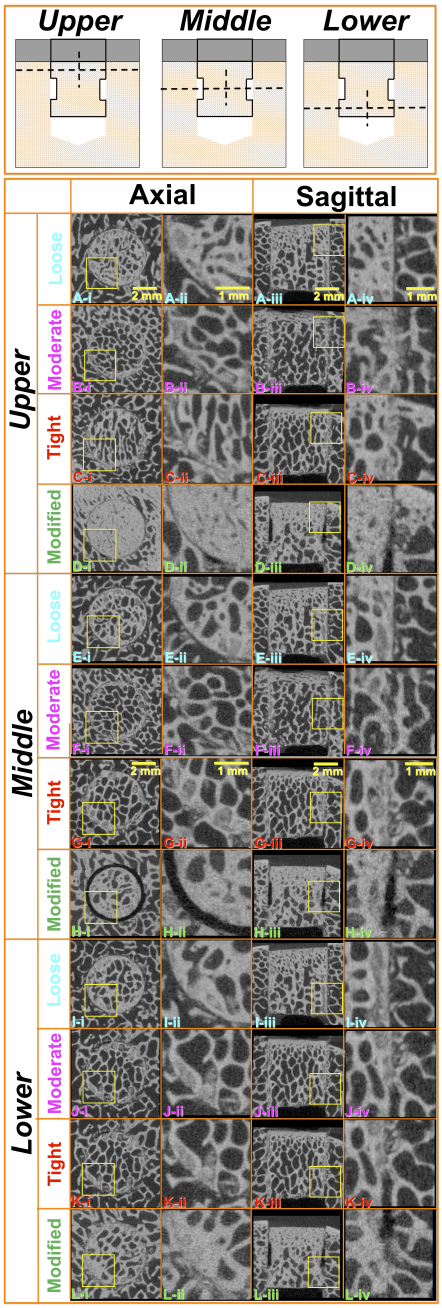

Figure 3.7 Qualitative µCT assessment of subchondral bone compaction at graft-host interface after OCG insertion. **(A-L)** µCT image slices were selected from **(A-D)** Upper, **(E-H)** Middle and **(I-L)** Lower portion of the graft-host subchondral bone interface, in **(i-ii)** Axial and **(iii-iv)** Sagittal orientations. Study Groups are standard OCG geometry with OCR that generate **(A, E, I)** Loose, **(B, F, J)** Moderate, and **(C, G, K)** Tight interference fits, and **(D, H, L)** Modified OCG geometry into OCR with tight fit. Yellow light box in **(i)** and **(iii)** indicates the zoom-in area of interest in **(ii)** and **(iv)**, respectively.

Table 3.1 Biomechanical parameters and variables.

parameter	definition	unit
A^{OCG}	articular cartilage surface area of OCG	mm^2
$h^{AC,OCG}$	thickness of AC of OCG prior to impact	mm

variable	definition	unit
a^{OCR}	radius of OCR	mm
$F(t)$	contact force applied on the tamp	N
$F_p[i]$	peak force applied on the tamp during tap #i	N
$I_c[i]$	impact impulse of the impact event of tap #i	N•ms
i	sequential tap # number to impact insert OCG into OCR, i=1,2,…,N	tap #
L_{crack}	total crack lengths on articular cartilage surface of OCG	mm
$T[i]$	impact time duration during tap #i	ms
t	relative timeframe for impact event	ms
$u_{adv}[i]$	OCG advancement distance during tap #i	mm
$u_{adv}[m]$	cumulative OCG advancement distance after tap #m	mm
$u^{Tamp}(t)$	axial displacement of the tamp	mm
$u_p^{AC,OCG}[i]$	peak axial compressive displacement of AC of OCG during tap #i	mm
$u_p^{Tamp}[i]$	peak axial displacement of the tamp during tap #i	mm
$V^{AC,OCG}$	surface chondrocyte viability of AC of OCG after insertion	%
W^{adv}	OCG advancement energy	mJ
$W^{adv}[i]$	OCG advancement energy during tap #i	mJ
$W^{AC,OCG}[i]$	energy delivered to AC of OCG during tap #i	mJ
$W_{insert}^{AC,OCG}$	total energy delivered to AC of OCG at completion of insertion	mJ
$W^{Tamp}[i]$	insertion energy delivered by the tamp to the sample during tap #i	mJ
$W^{Tamp}[m]$	cumulative insertion energy delivered by the tamp to the sample till tap #m	mJ
$W^{PE}[i]$	applied energy for tap #i	mJ
$\varepsilon_p[i]$	peak axial strain of AC of OCG during tap #i	mm/mm
$\sigma_p[i]$	peak contact stress during tap #i	MPa

Table 3.2 Effect of graft-host fit on biomechanics and biological outcomes among groups of: Loose (ΔR = 0.10mm), Moderate (ΔR = 0.05mm) and Tight (ΔR = 0.10mm). Statistical results are indicated as *** p<0.001, ** p<0.01, * p<0.05, with non-significant results presented with p value.

ΔR (mm)	n	tap #i	$W^{PE}[i]$ (mJ)	$F_p[i]$ (N)	$\sigma_p[i]$ (MPa)	$I_c[i]$ (N• ms)	$T[i]$ (ms)	$u_p^{Tamp}[i]$ (mm)	$u_{adv}[i]$ (mm)	$u_p^{AC,OCG}[i]$ (mm)	$\varepsilon_p[i]$	$W^{Tamp}[i]$ (mJ)	$W^{AC,OCG}[i]$ (mJ)	$W_{adv}[i]$ (mJ)
0.00	7	1	16	22 ±4	1.1 ±0.4	174 ±19	10.8 ±3.7	1.01 ±0.32	0.78 ±0.44	0.23 ±0.14	0.14 ±0.08	15.2 ±2.6	3.9 ±2.5	11.4 ±4.0
0.05	6	1	16	29 ±5	1.6 ±0.3	142 ±36	6.2 ±2.0	0.78 ±0.47	0.47 ±0.36	0.31 ±0.17	0.18 ±0.10	14.1 ±4.6	6.0 ±3.3	8.1 ±4.0
0.10	6	1	16	33 ±10	1.8 ±0.5	162 ±16	6.5 ±1.9	0.68 ±0.12	0.29 ±0.23	0.39 ±0.15	0.21 ±0.09	15.4 ±5.9	9.2 ±4.3	6.2 ±5.4
Effect of ΔR (p-value)				*	*	0.10	*	0.22	0.07	0.20	0.39	0.42	*	0.05
0.00	7	2	24	37 ±5	2.1 ±0.3	213 ±36	10.6 ±7.3	1.16 ±0.72	0.85 ±0.79	0.31 ±0.12	0.18 ±0.06	21.4 ±2.0	7.1 ±3.4	14.3 ±3.1
0.05	6	2	24	44 ±11	2.5 ±0.6	185 ±26	6.2 ±2.1	0.79 ±0.44	0.37 ±0.32	0.43 ±0.18	0.25 ±0.11	21.3 ±6.5	11.6 ±3.2	9.7 ±6.8
0.10	6	2	24	56 ±10	3.1 ±0.6	202 ±19	4.8 ±1.3	0.63 ±0.09	0.14 ±0.09	0.49 ±0.09	0.26 ±0.06	23.7 ±2.7	18.7 ±4.7	5.1 ±2.7
Effect of ΔR (p-value)				**	**	0.24	0.09	0.18	0.07	0.08	0.17	0.74	**	**
0.00	7	3	36	51 ±10	2.8 ±0.5	232 ±34	8.0 ±1.7	1.07 ±0.13	0.73 ±0.13	0.35 ±0.07	0.21 ±0.03	30.5 ±4.7	9.9 ±2.5	20.6 ±3.9
0.05	6	3	36	61 ±16	3.4 ±0.9	220 ±21	5.3 ±0.8	0.79 ±0.16	0.41 ±0.14	0.38 ±0.12	0.22 ±0.07	29.7 ±2.7	14.3 ±4.0	15.5 ±4.5
0.10	6	3	36	79 ±15	4.4 ±0.9	244 ±38	3.8 ±0.9	0.66 ±0.11	0.17 ±0.10	0.48 ±0.12	0.26 ±0.08	35.4 ±8.6	26.6 ±10.4	8.7 ±5.2
Effect of ΔR (p-value)				**	**	0.45	***	***	***	0.10	0.35	0.15	**	***
0.00	6	4	54	69 ±25	3.8 ±1.4	251 ±45	6.1 ±2.0	1.30 ±0.35	0.89 ±0.34	0.42 ±0.23	0.24 ±0.11	35.4 ±17.5	10.3 ±7.8	25.0 ±13.9
0.05	6	4	54	77 ±16	4.3 ±0.9	246 ±18	4.6 ±1.1	0.85 ±0.18	0.43 ±0.17	0.42 ±0.09	0.24 ±0.06	41.8 ±2.3	20.8 ±4.0	21.0 ±5.6
0.10	6	4	54	95 ±17	5.2 ±0.9	267 ±51	3.4 ±0.8	0.68 ±0.11	0.17 ±0.09	0.51 ±0.12	0.27 ±0.06	43.9 ±8.0	33.5 ±10.3	10.4 ±5.6
Effect of ΔR (p-value)				0.10	0.10	0.65	*	**	**	0.54	0.76	0.53	***	***
0.00	4	5	81	92 ±39	5.1 ±2.2	326 ±23	5.6 ±2.6	1.18 ±0.38	0.58 ±0.45	0.60 ±0.29	0.37 ±0.20	65.4 ±11.2	36.3 ±18.9	29.1 ±11.9
0.05	6	5	81	100 ±21	5.5 ±1.1	292 ±46	4.2 ±1.6	0.93 ±0.26	0.49 ±0.30	0.44 ±0.10	0.25 ±0.06	60.5 ±11.0	29.7 ±10.2	30.8 ±13.6
0.10	6	5	81	122 ±21	6.7 ±1.1	333 ±42	3.3 ±0.4	0.83 ±0.09	0.19 ±0.06	0.64 ±0.11	0.34 ±0.07	74.7 ±11.8	57.5 ±13.5	17.1 ±4.9
Effect of ΔR (p-value)				0.20	0.20	0.22	0.21	0.13	0.11	0.14	0.23	0.19	*	0.13
0.05	6	6	122	130 ±28	7.2 ±1.5	354 ±25	4.3 ±1.2	1.14 ±0.18	0.63 ±0.22	0.51 ±0.12	0.29 ±0.07	89.4 ±11.2	41.7 ±17.5	47.7 ±10.0
0.10	6	6	122	147 ±24	8.1 ±1.3	401 ±42	3.4 ±0.8	0.98 ±0.09	0.40 ±0.22	0.58 ±0.22	0.31 ±0.11	106.2 ±12.8	65.0 ±30.7	41.2 ±19.7
Effect of ΔR (p-value)				0.29	0.29	*	0.29	0.08	0.10	0.51	0.72	*	0.14	*
0.05	5	7	183	175 ±12	9.7 ±0.6	478 ±32	4.6 ±1.6	1.39 ±0.26	0.92 ±0.32	0.47 ±0.23	0.27 ±0.14	138.4 ±21.2	50.1 ±29.6	88.3 ±11.5
0.10	6	7	183	175 ±31	9.7 ±1.7	450 ±40	3.5 ±1.2	1.16 ±0.21	0.53 ±0.31	0.64 ±0.21	0.34 ±0.12	136.4 ±21.1	80.1 ±42.5	56.2 ±23.4
Effect of ΔR (p-value)				1.00	1.00	0.24	0.34	0.14	0.07	0.23	0.61	0.79	0.26	0.36
0.05	2	8	274	282 ±28	15.6 ±1.5	609 ±16	2.8 ±0.7	1.35 ±0.12	0.48 ±0.22	0.87 ±0.10	0.54 ±0.04	272.9 ±42.4	179.7 ±63.6	93.2 ±21.2
0.10	6	8	274	220 ±40	12.2 ±2.2	573 ±68	3.7 ±1.2	1.53 ±0.35	0.62 ±0.34	0.91 ±0.29	0.48 ±0.15	226.0 ±36.5	142.4 ±62.8	83.6 ±32.5
Effect of ΔR (p-value)				0.09	0.09	0.51	0.37	0.52	0.61	0.86	0.61	0.17	0.08	0.26
0.10	4	9	411	327 ±35	18.1 ±1.9	695 ±61	3.0 ±1.0	1.51 ±0.27	0.70 ±0.31	0.81 ±0.31	0.45 ±0.23	349.7 ±44.5	190.9 ±94.5	158.8 ±65.8
0.10	3	10	617	377 ±70	20.8 ±3.9	871 ±56	2.7 ±0.9	1.80 ±0.58	0.74 ±0.64	1.05 ±0.16	0.61 ±0.20	498.8 ±29.8	317.1 ±129.4	181.8 ±106.1
0.10	2	11	925	434 ±110	24.0 ±6.1	1002 ±90	2.9 ±1.0	2.08 ±0.68	1.22 ±0.83	0.86 ±0.15	0.56 ±0.11	642.0 ±145.1	304.0 ±205.8	337.9 ±60.7
0.10	1	12	1387	843	46.6	1508	1.9	1.82	1.00	0.82	0.53	1427.9	642.4	785.5

Table 3.3 Effect of OCG geometry modification on biomechanics and biological outcomes. *Mod.*: OCG geometry modification. Statistical results are indicated as *** p<0.001, ** p<0.01, * p<0.05, with non-significant results presented with p value.

ΔR [mm]	OCG Mod.	n	tap #i	$W^{PE}[i]$ (mJ)	$F_p[i]$ (N)	$\sigma_p[i]$ (MPa)	$I_c[i]$ (N•ms)	$T[i]$ (ms)	$u_p^{Tamp}[i]$ (mm)	$u_{adv}[i]$ (mm)	$u_p^{AC,OCG}[i]$ (mm)	$\varepsilon_p[i]$	$W^{Tamp}[i]$ (mJ)	$W^{AC,OCG}[i]$ (mJ)	$W_{adv}[i]$ (mJ)
0.10	−	6	1	16	33 ±10	1.8 ±0.5	162 ±16	6.5 ±1.9	0.68 ±0.12	0.29 ±0.23	0.39 ±0.15	0.21 ±0.09	15.4 ±5.9	9.2 ±4.3	6.2 ±5.4
0.10	+	7	1	16	36 ±5	2.0 ±0.3	173 ±10	6.3 ±1.7	0.55 ±0.12	0.24 ±0.12	0.31 ±0.15	0.21 ±0.09	14.5 ±2.6	8.2 ±3.9	6.3 ±3.3
Effect of *Mod.* (p-value)					0.50	0.50	0.16	0.84	0.08	0.62	0.36	1.00	0.42	1.00	0.15
0.10	−	6	2	24	56 ±10	3.1 ±0.6	202 ±19	4.8 ±1.3	0.63 ±0.09	0.14 ±0.09	0.49 ±0.09	0.26 ±0.06	23.7 ±2.7	18.7 ±4.7	5.1 ±2.7
0.10	+	7	2	24	55 ±12	3.0 ±0.7	195 ±38	4.0 ±4.0	0.60 ±0.20	0.29 ±0.12	0.32 ±0.16	0.21 ±0.08	22.8 ±3.6	12.2 ±4.2	10.6 ±2.6
Effect of *Mod.* (p-value)					0.87	0.87	0.69	0.65	0.74	*	*	0.24	1.00	0.05	0.81
0.10	−	6	3	36	79 ±15	4.4 ±0.9	244 ±38	3.8 ±0.9	0.66 ±0.11	0.17 ±0.10	0.48 ±0.12	0.26 ±0.08	35.4 ±8.6	26.6 ±10.4	8.7 ±5.2
0.10	+	7	3	36	72 ±20	4.0 ±1.1	259 ±22	5.9 ±3.3	0.91 ±0.61	0.47 ±0.67	0.44 ±0.23	0.29 ±0.13	36.3 ±2.8	21.1 ±12.8	14.3 ±11.8
Effect of *Mod.* (p-value)					0.50	0.50	0.39	0.16	0.35	0.30	0.71	0.63	1.00	0.43	0.22
0.10	−	6	4	54	95 ±17	5.2 ±0.9	267 ±51	3.4 ±0.8	0.68 ±0.11	0.17 ±0.09	0.51 ±0.12	0.27 ±0.06	43.9 ±8.0	33.5 ±10.3	10.4 ±5.6
0.10	+	7	4	54	85 ±19	4.7 ±1.0	266 ±51	4.4 ±1.5	0.72 ±0.15	0.34 ±0.15	0.38 ±0.23	0.25 ±0.13	40.5 ±5.5	21.0 ±11.1	19.5 ±8.0
Effect of *Mod.* (p-value)					0.34	0.34	0.97	0.17	0.60	0.26	0.24	0.74	0.33	*	0.20
0.10	−	6	5	81	122 ±21	6.7 ±1.1	333 ±42	3.3 ±0.4	0.83 ±0.09	0.19 ±0.06	0.64 ±0.11	0.34 ±0.07	74.7 ±11.8	57.5 ±13.5	17.1 ±4.9
0.10	+	7	5	81	103 ±14	5.7 ±0.8	312 ±62	4.6 ±1.2	0.96 ±0.22	0.51 ±0.31	0.45 ±0.15	0.31 ±0.10	60.4 ±9.1	31.1 ±19.2	29.3 ±16.2
Effect of *Mod.* (p-value)					0.08	0.08	0.50	0.08	0.21	*	*	0.55	*	*	*
0.10	−	6	6	122	147 ±24	8.1 ±1.3	401 ±42	3.4 ±0.8	0.98 ±0.09	0.40 ±0.22	0.58 ±0.22	0.31 ±0.11	106.2 ±12.8	65.0 ±30.7	41.2 ±19.7
0.10	+	6	6	122	120 ±21	6.6 ±1.2	377 ±41	5.0 ±1.2	1.34 ±0.33	1.00 ±0.32	0.34 ±0.13	0.22 ±0.07	84.6 ±12.5	22.0 ±8.4	62.6 ±11.8
Effect of *Mod.* (p-value)					0.06	0.06	0.34	0.06	*	**	*	0.12	*	**	**
0.10	−	6	7	183	175 ±31	9.7 ±1.7	450 ±40	3.5 ±1.2	1.16 ±0.21	0.53 ±0.31	0.64 ±0.21	0.34 ±0.12	136.4 ±21.1	80.1 ±42.5	56.2 ±23.4
0.10	+	6	7	183	154 ±28	8.5 ±1.6	465 ±49	4.4 ±1.3	1.27 ±0.26	0.82 ±0.20	0.45 ±0.11	0.29 ±0.06	122.1 ±7.7	43.2 ±8.8	78.9 ±9.5
Effect of *Mod.* (p-value)					0.25	0.25	0.57	0.24	0.44	0.08	0.08	0.38	0.21	0.09	0.17
0.10	−	6	8	274	220 ±40	12.2 ±2.2	573 ±68	3.7 ±1.2	1.53 ±0.35	0.62 ±0.34	0.91 ±0.29	0.48 ±0.15	226.0 ±36.5	142.4 ±62.8	83.6 ±32.5
0.10	+	3	8	274	219 ±63	12.1 ±3.5	575 ±117	3.6 ±1.4	1.42 ±0.28	0.85 ±0.31	0.57 ±0.47	0.36 ±0.26	180.0 ±22.3	72.2 ±60.5	107.9 ±38.2
Effect of *Mod.* (p-value)					0.98	0.98	0.97	0.91	0.65	0.36	0.21	0.40	0.09	0.15	0.42
0.10	−	4	9	411	327 ±35	18.1 ±1.9	695 ±61	3.0 ±1.0	1.51 ±0.27	0.70 ±0.31	0.81 ±0.31	0.45 ±0.23	349.7 ±44.5	190.9 ±94.5	158.8 ±65.8
0.10	+	2	9	411	215 ±42	11.9 ±2.3	666 ±125	3.8 ±0.0	1.71 ±0.38	0.80 ±0.75	0.92 ±0.36	0.58 ±0.16	269.1 ±13.2	152.1 ±84.0	117.0 ±97.2
Effect of *Mod.* (p-value)					*	*	0.70	n/a	0.49	0.81	0.71	0.52	0.08	0.64	0.12
0.10	−	3	10	617	377 ±70	20.8 ±3.9	871 ±56	2.7 ±0.9	1.80 ±0.58	0.74 ±0.64	1.05 ±0.16	0.61 ±0.20	498.8 ±29.8	317.1 ±129.4	181.8 ±106.1
0.10	+	1	10	617	301	16.6	801	3.6	1.93	0.91	1.02	0.60	431.4	228.3	203.1
Effect of *Mod.* (p-value)					n/a	n/a	n/a	n/a	n/a	n/a	n/a	n/a	n/a	n/a	n/a
0.10	−	2	11	925	434 ±110	24.0 ±6.1	1002 ±90	2.9 ±1.0	2.08 ±0.68	1.22 ±0.83	0.86 ±0.15	0.60	642.0 ±145.1	304.0 ±205.8	337.9 ±60.7
0.10	−	1	12	1387	843	46.6	1508	1.9	1.82	1.00	0.82	0.53	1427.9	642.4	785.5

3.7 References

1. Hangody L, Vasarhelyi G, Hangody LR, Sukosd Z, Tibay G, Bartha L, Bodo G. Autologous osteochondral grafting--technique and long-term results. *Injury.* 2008;39 Suppl 1:S32-39.

2. Cole BJ, Pascual-Garrido C, Grumet RC. Surgical management of articular cartilage defects in the knee. *J Bone Joint Surg Am.* 2009;91(7):1778-1790.

3. Borazjani BH, Chen AC, Bae WC, Patil S, Sah RL, Firestein GS, Bugbee WD. Effect of impact on chondrocyte viability during the insertion of human osteochondral grafts. *J Bone Joint Surg Am.* 2006;88:1934-1943.

4. Pallante-Kichura AL, Cory E, Bugbee WD, Sah RL. Bone cysts after osteochondral allograft repair of cartilage defects in goats suggest abnormal interaction between subchondral bone and overlying synovial joint tissues. *Bone.* 2013;57:259–268.

5. Pallante AL, Chen AC, Ball ST, Amiel D, Masuda K, Sah RL, Bugbee WD. The in vivo performance of osteochondral allografts in the goat is diminished with extended storage and decreased cartilage cellularity. *Am J Sports Med.* 2012;40:1814-1823.

6. Whiteside RA, Jakob RP, Wyss UP, Mainil-Varlet P. Impact loading of articular cartilage during transplantation of osteochondral autograft. *J Bone Joint Surg Br.* 2005;87:1285-1291.

7. Pylawka TK, Wimmer M, Cole BJ, Virdi AS, Williams JM. Impaction affects cell viability in osteochondral tissues during transplantation. *J Knee Surg.* 2007;20:105-110.

8. Patil S, Butcher W, D'Lima DD, Steklov N, Bugbee WD, Hoenecke HR. Effect of osteochondral graft insertion forces on chondrocyte viability. *Am J Sports Med.* 2008;36(9):1726-1732.

9. Kock NB, van Susante JL, Wymenga AB, Buma P. Press-fit stability of an osteochondral autograft: Influence of different plug length and perfect depth alignment. *Acta Orthop.* 2006;77:422-428.

10. Repo RU, Finlay JB. Survival of articular cartilage after controlled impact. *J Bone Joint Surg Am.* 1977;59-A:1068-1076.

11. Torzilli PA, Grigiene R, Borrelli J, Jr., Helfet DL. Effect of impact load on articular cartilage: cell metabolism and viability, and matrix water content. *J Biomech Eng.* 1999;121:433-441.

12. Ewers BJ, Dvoracek-Driksna D, Orth MW, Haut RC. The extent of matrix damage and chondrocyte death in mechanically traumatized articular cartilage explants depends on rate of loading. *J Orthop Res.* 2001;19:779-784.

13. Milentijevic D, Torzilli PA. Influence of stress rate on water loss, matrix deformation and chondrocyte viability in impacted articular cartilage. *J Biomech.* 2005;38:493-502.

14. Torzilli PA, Deng XH, Ramcharan M. Effect of compressive strain on cell viability in statically loaded articular cartilage. *Biomech Model Mechanobiol.* 2006;5(2-3):123-132.

15. Quinn TM, Allen RG, Schalet BJ, Perumbuli P, Hunziker EB. Matrix and cell injury due to sub-impact loading of adult bovine articular cartilage explants: effects of strain rate and peak stress. *J Orthop Res.* 2001;19:242-249.

16. Szczodry M, Coyle CH, Kramer SJ, Smolinski P, Chu CR. Progressive chondrocyte death after impact injury indicates a need for chondroprotective therapy. *Am J Sports Med.* 2009;37(12):2318-2322.

17. Finlay JB, Repo RU. Energy absorbing ability of articular cartilage during impact. *Med Biol Eng Comput.* 1979 17:397-403.

18. Burgin LV, Aspden RM. Impact testing to determine the mechanical properties of articular cartilage in isolation and on bone. *J Mater Sci Mater Med.* 2008 19:703-711.

19. Salem SA, Al-Hassani ST, Johnson W. Aspects of the mechanics of driving nails into wood. *Int J Mech Sci.* 1975;17:211-225.

20. Selvage CC. *Assembly of interference fits by impact and constant force methods*, Massachusetts Institute of Technology; 1979.

21. Rho JY, Ashman RB, Turner CH. Young's modulus of trabecular and cortical bone material: ultrasonic and microtensile measurements. *J Biomech.* 1993;26:111-119.

22. Schinagl RM, Gurskis D, Chen AC, Sah RL. Depth-dependent confined compression modulus of full-thickness bovine articular cartilage. *J Orthop Res.* 1997;15:499-506.

23. Korhonen RK, Laasanen MS, Toyras J, Rieppo J, Hirvonen J, Helminen HJ, Jurvelin JS. Comparison of the equilibrium response of articular cartilage in unconfined compression, confined compression and indentation. *J Biomech.* 2002;35(7):903-909.

24. Choi K, Kuhn JL, Ciarelli MJ, Goldstein SA. The elastic moduli of human subchondral, trabecular, and cortical bone tissue and the size-dependency of cortical bone modulus. *J Biomech.* 1990;23:1103-1113.

25. Shepherd DET, Seedhom BB. The 'instantaneous' compressive modulus of human articular cartilage in joints of the lower limb. *Rheumatology (Oxford).* 1999;38:124-132.

26. Hurtig M, Buschmann MD, Fortier L, Hoemann CD, Hunziker EB, Jurvelin JS, Mainil-Varlet P, McIlwraith CW, Sah RL, Whiteside RA. Preclinical studies for cartilage repair: recommendations from the International Cartilage Repair Society. *Cartilage.* 2011;2(2):137-152.

27. Chu CR, Szczodry M, Bruno S. Animal models for cartilage regeneration and repair. *Tissue Eng Part B Rev.* 2010;16(1):105-115.

28. Barber FA, Herbert MA, McGarry JE, Barber CA. Insertion force of articular cartilage transplant systems. *J Knee Surg.* 2008;21:200-204.

29. Claes L, Augat P, Suger G, Wilke HJ. Influence of size and stability of the osteotomy gap on the success of fracture healing. *Journal of Orthopaedic Research.* 1997;15(4):577-584.

30. Duchow J, Hess T, Kohn D. Primary stability of press-fit-implanted osteochondral grafts. *Am J Sports Med.* 2000;28:24-27.

CHAPTER 4

CONCLUSIONS

4.1 Summary of Findings

This dissertation developed an innovative approach to study OCG impact insertion and achieved the goals of: (a) extending the understanding of OCG insertion biomechanics and its mechanobiological consequences, (b) developing potential strategies to decrease impact injury to graft cartilage during OCG insertion surgery. In Summary, the novel methodologies taken in this dissertation are:

(A) Development of an impact delivery system using a drop tower apparatus, with force and displacement measurements during impact to quantify biomechanical variables (**Chapter 2**).

(B) Development of an *ex vivo* large animal (adult bovine) model to study OCG insertion biomechanics and the effect of graft-host interference fit as well as OCG geometry modification (**Chapter 3**).

(C) Use of a cushioning material to alter impact energy partitioning, as an analogous model to study traumatic injury to articular cartilage (**Chapter 2**).

The major findings corresponding to the scientific objectives were:

1. Delivered energy is a critical biomechanical determinant of damage to articular cartilage during OCS impact and OCG insertion.
2. Tighter graft-host interference fit leads to higher insertion energy and more resultant surface chondrocyte death as well as matrix damage to the graft cartilage.
3. Modification of OCG subchondral bone geometry results in less insertion energy with less chondrocyte death and matrix damage.
4. Inclusion of a cushioning material during impact lessens impact energy delivered to OCS and the resultant damage to cartilage.

4.2 Discussion and Future Directions

This dissertation was motivated by the attempt to solve biomechanical problems of OCG insertion repair. The results in this work contribute novel and important information for future improvement of the surgical procedure and instrument design. A broader application of the impact delivery system includes *ex vivo* models to study traumatic injury to the joint, and its potential translation into the mechanobiology of post-traumatic osteoarthritis *in vivo*.

Certain limitations of the work should be considered. First, the geometry of OCG was smaller than that used clinically in order to generate reasonable numbers of samples for statistical purposes. The depth of OCR was almost twice as long as the allogenic OCG, although similar to that of autogenic OCG in current surgical practice [1, 2]. Second, Adult bovine osteochondral tissue is not identical to that of human in terms of cartilage thickness and material properties, and bone structure and properties. Third, in the clinical scenario, the surgeon typically applies taps manually, instead of using a preset impact load protocol. This dissertation utilized bovine tissue to validate the experimental methodologies to approach the scientific problems of OCG insertion.

The current work can be expanded in a number of ways toward future clinical translation. Human osteochondral tissues could be analyzed, with the size and geometry of the OCG and OCR being analogous to those in actual autogenic or allogenic surgery. The insertion process could be done by independent surgeons to better determine the effect of graft-host fit and OCG geometry modification in real surgery.

"Bottoming out" of OCG can happen because current surgical procedure does not intend to leave gaps underneath the OCG after insertion. In this situation, *ex vivo*

instrument-controlled studies can facilitate characterization of the biomechanics and consequent effect on graft cartilage health at the end of the insertion process, although these can be partially inferred from results of impacting isolated OCS without insertion.

The concept of altering impact insertion biomechanics gave rise to the idea of OCG geometry modification to reduce damage to graft cartilage while maintaining mechanical stability and biological integration propensity. The same concept can be further extended for alternative designs to decrease insertion energy, such as modifying the socket wall of OCR, or altering the OCG subchondral bone in shape, depth and length. Modifications that lead to empty space at the graft-host interface may be deleterious to graft-host-healing, due to less subchondral bone contact area as well as potentially higher risk of fluid accumulation and subsequent bone cyst formation.

The effect of graft-host interference fit on graft stability after insertion has not been reported in the literature. This issue can be addressed acutely by assessing graft failure after applying repetitive axial and shearing loads on flush-inserted grafts with different tightness of fit, and with subchondral bone geometry modification. Related to this, the base of the OCG can affect "bottoming out" and be another variable affecting graft stability.

Quantitative analysis of μCT images can facilitate the experimental understanding of the mechanics behind the effects of graft-host interference fit. In addition to qualitative observation, quantifying the extent of subchondral bone impaction, including features such as deformation and trabecular fracture, may provide valuable information to further solve insertion energy problems.

The impact delivery system can be expanded to setup an *ex vivo* model to study orthopaedic trauma to synovial joints. The cushioning material serves as an additional component in the system to partition the impact energy, analogous to the counteraction or interposition of soft tissues in sports injury or accidental trauma. Such a system could be modified to deliver impact energy to osteochondral tissues of larger size, with multiple options of the cushion to mimic various scenarios of energy distribution.

In conclusion, OCG insertion repair surgery involves OCG and OCR preparation, OCG insertion process and graft stability after insertion. Each of the steps can play an important role in the long-term outcome of the patient. Taken together, this dissertation focused on the OCG insertion process and provided a foundation for additional investigation of this situation and related problems in the future.

4.3 References

1. Cole BJ, Pascual-Garrido C, Grumet RC. Surgical management of articular cartilage defects in the knee. *J Bone Joint Surg Am*. 2009;91(7):1778-1790.

2. Alford JW, Cole BJ. Cartilage restoration, part 2: techniques, outcomes, and future directions. *Am J Sports Med*. 2005;33(3):443-460.